*Journal of Marine Research, 55,* 117–151, 1997

# Analysis of the mean annual cycle of the dissolved oxygen anomaly in the World Ocean

by Raymond G. Najjar[1] and Ralph F. Keeling[2]


## ABSTRACT

A global climatology of the dissolved oxygen anomaly (the excess over saturation) is created with monthly resolution in the upper 500 m of the ocean. The climatology is based on dissolved oxygen, temperature and salinity data archived at the National Oceanographic Data Center. Examination of this climatology reveals statistically significant annual cycles throughout the upper 500 m of the World Ocean, though seasonal variations are most coherent in the North Atlantic, where data density is greatest.

Vertical trends in the phase and amplitude of the annual cycle are noted. The cycle in surface waters is characterized by a summer maximum and a winter minimum, consistent with warming and high rates of photosynthesis during the summer, and cooling and entrainment of oxygen-depleted water during the winter. In low and middle latitudes, the amplitude increases with depth and the maximum occurs later in the year, a trend consistent with the seasonal accumulation of oxygen associated with the shallow oxygen maximum. At a depth that varies between about 30 and 130 m, the phase of the annual cycle undergoes an abrupt shift. We call this depth the *oxygen nodal depth.* Below the nodal depth, the annual cycle is characterized by an early-spring maximum and a late-fall minimum, consistent with a cycle dominated by respiration during the spring and summer and replenishment of oxygen from the atmosphere by ventilation during the fall and winter. Below the nodal depth, the amplitude of the annual cycle generally decreases with depth, indicative of decreasing respiration and ventilation rates, or less seasonality in both processes. We postulate that the nodal depth in middle and high latitudes corresponds closely to the summertime compensation depth, where photosynthesis and net community respiration are equal. With this interpretation of the nodal depth and a simple model of the penetration of light in the water column, a compensation light intensity of 1 W $m^{-2}$ (4 $\mu E$ $m^{-2}$ $s^{-1}$) is deduced, at the low end of independent estimates.

Horizontal trends in the phase and amplitude of the annual cycle are also noted. We find that the nodal depth decreases toward the poles in both hemispheres and is generally greater in the Southern Hemisphere, patterns found to be consistent with light-based estimates of the compensation depth. The amplitude of the annual cycle in the oxygen anomaly increases monotonically with latitude, and higher latitudes lag lower latitudes. In the North Atlantic and North Pacific, the amplitude of the annual cycle tends to increase from east to west at all depths and latitudes, as expected considering that physical forcing has greater seasonal variability in the west.

The tropics and the North Indian Ocean have features that distinguish them from other regions. Below about 75 m, these waters have pronounced annual cycles of the oxygen anomaly that are


1. The Pennsylvania State University, Department of Meteorology, 503 Walker Building, University Park, Pennsylvania, 16802-5013, U.S.A.

2. Scripps Institution of Oceanography, 9500 Gilman Drive, La Jolla, California, 92093-0236, U.S.A.

shown to be caused mainly by wind-driven adiabatic displacements of the thermocline. A semiannual cycle of the oxygen anomaly is found in the surface waters of the North Indian Ocean, consistent with the known semiannual cycle of surface heat flux in this region.

## 1. Introduction

Studies of the annual cycle of oxygen have provided great insight into the biogeochemical dynamics of the upper ocean and have put powerful constraints on the rates of biological production and air-sea gas exchange, two processes of paramount importance to marine biogeochemistry (Redfield, 1948; Shulenberger and Reid, 1981; Jenkins and Goldman, 1985; Emerson, 1987; Spitzer and Jenkins, 1989). Nevertheless, the annual cycle of oxygen has been studied at only a small set of deep-water locations restricted to the North Atlantic and North Pacific: the Sargasso Sea (Jenkins and Goldman, 1985; Michaels *et al.,* 1994); the Subarctic Atlantic (Peng *et al.,* 1987); the Eastern Subarctic Pacific (Reid, 1962; Tabata, 1965; Emerson, 1987); the Central Subtropical North Pacific (Emerson *et al.,* 1993; Bingham and Lukas, 1996); offshore of Washington and Oregon (Stefánsson and Richards, 1964); offshore of Southern California (Reid, 1962; Hayward, 1994); and offshore of Japan (Okubo, 1959; Reid, 1962; Suga and Hanawa, 1990).

Here we draw on the extensive set of historical oxygen measurements at the National Oceanographic Data Center (NODC) to create a global ocean climatology of the mean annual cycle of the dissolved oxygen anomaly ($\Delta[O_2]$, the excess over saturation). Our hope is that this climatology will aid in the task of understanding the ocean's role in global biogeochemical cycles by providing a new basis for the estimation of large-scale marine biological production, remineralization and gas-exchange rates. We anticipate that the climatology will also be helpful in evaluating numerical models of marine biogeochemistry and will provide a valuable complement to regional oceanic studies, and to studies of the variability of oxygen in the atmosphere (Keeling and Shertz, 1992).

In the next section, we synthesize some of the previous research on the annual cycle of oxygen in the ocean and present a canonical midlatitude annual oxygen cycle. This synthesis will serve as a framework for the discussion of our results. In Section 3, we briefly summarize the methods for creating the climatology, relegating the details to the Appendix. In Sections 4 and 5, we present the climatology and provide largely qualitative explanations for what we see. Because of the variable quality and limited spatial and temporal coverage of the NODC data set, some of our analyses may have errors as large as the signals of interest, particularly on small spatial and temporal scales. Recognizing these difficulties, we have limited our discussion to general features that appear to be resolved reliably, such as spatial patterns evident in summer/winter differences, and trends evident in the first harmonic of the zonal-mean cycles.

## 2. Background

The annual cycle of oxygen in the ocean varies in character depending on depth. Four distinct cycles have been noted (Fig. 1) and are separated vertically by the depth of the

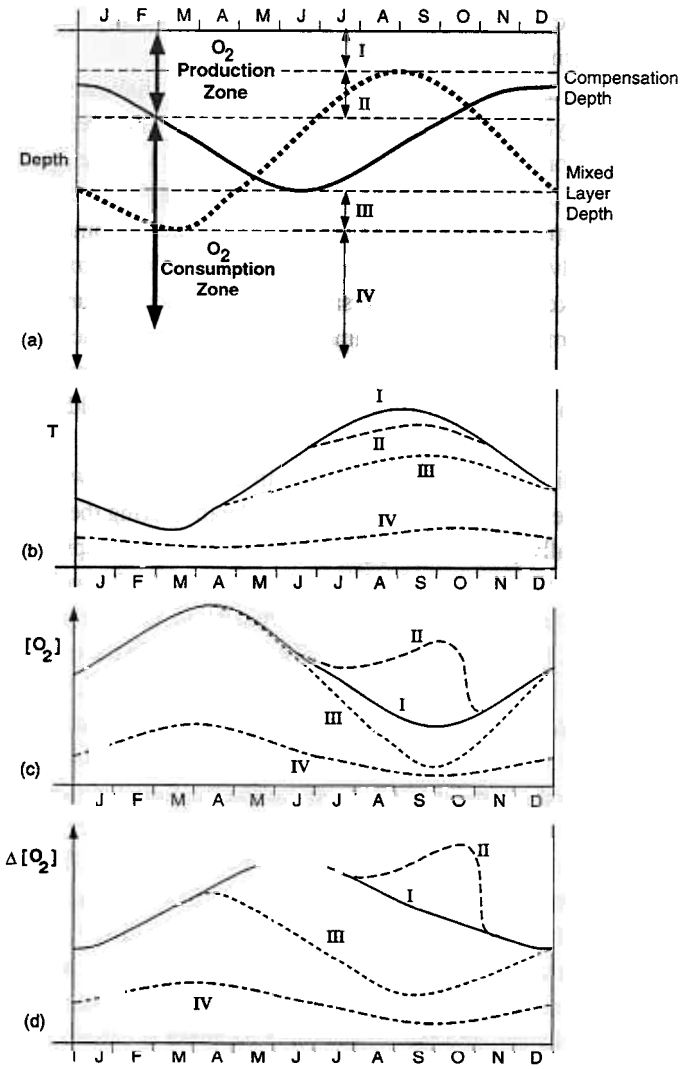


Figure 1. Schematic diagram illustrating the four annual oxygen cycles in extra-tropical waters of the Northern Hemisphere. (a) Mixed layer depth, compensation depth and the location of the four zones; (b) temperature, (c) oxygen and (d) oxygen anomaly cycle in the four zones.

shallowest mixed layer, the depth of the deepest mixed layer and the summertime compensation depth. For our purposes, the compensation depth is defined such that the biological community is a net source of oxygen above the compensation depth and a net sink of oxygen below the compensation depth, a definition consistent with the ideas of Sverdrup (1953) and Smetacek and Passow (1990). The compensation depth probably has an annual cycle in open ocean water that is largely driven by the solar flux at the surface. In

other words, we expect the compensation depth to be greatest in the early summer and smallest in the early winter.

First consider the shallowest annual cycle, that above the shallowest mixed layer depth. Within the mixed layer, oxygen is often very close to the (temperature-dependent) saturation concentration. Oxygen is therefore out of phase with temperature, the lowest concentrations being reached in late summer and the highest in late winter (Reid, 1962). Slight departures from saturation result, in part, from net community $O_2$ production, surface heat fluxes, advection and turbulent diffusion, injection of oxygen by bubbles and the finite rate of gas exchange. High supersaturation often occurs during the early summer when the rates of warming and net community production are highest. During the winter, surface cooling and the entrainment of low-oxygen water due to mixed-layer deepening lead to undersaturation or very low supersaturation (Jenkins and Goldman, 1985; Emerson, 1987).

A second, slightly different annual cycle exists in the waters below the shallowest mixed layer but still above the summertime compensation depth. During the summer in this depth range, photosynthetically-produced oxygen is prevented from escaping to the atmosphere by the stable seasonal thermocline. Such conditions result in the well-known subsurface oxygen maximum, a feature which is most prominent in the late summer (Reid, 1962; Jenkins and Goldman, 1985; Hayward, 1994). Thus the cycle in the oxygen anomaly at this depth lags the surface cycle during the summer. Starting in the fall, when the mixed layer begins to deepen, the high $O_2$ water is diluted with the overlying water above and the cycle then becomes similar to the surface cycle, a situation that prevails until the mixed layer shoals and rises above the compensation depth during the following spring and summer.

In contrast to these two "production zone" cycles, the annual cycles of oxygen in the deeper "consumption zone" have received very little attention. Rakestraw and Carritt (1948) reported an annual oxygen cycle in the Sargasso Sea at 300 m, with oxygen highest in the late winter and lowest in the late summer. Worthington (1959) interpreted these data as a ventilation-respiration cycle: the wintertime increase occurs when the mixed layer deepens and imposes surface characteristics—including higher oxygen concentrations—on the deeper layers, and the summertime decrease is caused by respiration in the absence of significant mixing below the shoaled mixed layer.

A fourth, similar type of oxygen cycle was proposed by Jenkins (1982) and Jenkins and Goldman (1985) in studies of the extensive time series of oxygen measurements in the Sargasso Sea at Station S. They reported an annual cycle between 100 and 400 m similar to Rakestraw and Carritt's, but argued that the deeper layers must be ventilated laterally at outcrops to the north, not vertically by the mixed layer above. Jenkins (1982) and Jenkins and Goldman (1985) also noted a lag and a decreasing amplitude with depth, which they attributed to decreases in ventilation and respiration rates with depth.

Consumption zone cycles are also present in the analyses of North Pacific time series. Reid (1962) presented figures of the mean annual cycle of the oxygen concentration and percent saturation at stations off the coasts of Japan and Southern California, all of which

show clear spring maxima and fall minima between about 75 and 150 m. The origin and significance of the cycles was not discussed, however. Also, Tabata (1964) found that the oxygen concentration at 75 and 100 m depth at Station P (50N, 145W) decreased from May through November and he attributed this to entrainment of water from the halocline.

We can find no other mention of consumption-zone oxygen cycles in the literature, except for the recent atlas of Levitus and Boyer (1994a), who analyzed oxygen from the NODC archives and from the results of a data archaeology program to create four seasonal analyses. It is surprising that more notice has not been made of the annual oxygen cycle in the consumption zone, especially given the large number of oxygen measurements that have been made and of the central role of the oxygen utilization rate in a variety of oceanographic studies. We suspect that the lack of time series measurements, such as those at the former ocean weather stations, have made it difficult to extract the annual cycle from measurements that are synoptic in nature and made by many different investigators, often with different measurement protocols and quality control. Even at time series stations, the annual cycle in the consumption zone is not readily evident until the data are averaged by month, indiscriminate of year (Jenkins, 1982; Jenkins and Goldman, 1985). It is likely then, that interannual and mesoscale variability significantly obscure the annual oxygen cycle in the consumption zone, although, as shown below, this cycle is a general feature of the World Ocean at middle and high latitudes.

## 3. Methods

### *a. Overview of the data set*

The data set used in this study is the Oceanographic Station Data of the NODC as of March 1994, and contains more than 880,000 stations, about one third of which contain at least one oxygen measurement. The distribution of these oxygen stations reveals the expected high density in the Northern Hemisphere and in coastal waters (Fig. 2). Though the data set spans from 1898 to 1991, most of the measurements are from the 1960s and 70s. Fifty two countries have contributed oxygen measurements to this data set, though three of them have contributed 57% of the oxygen stations: the United States (26%), the Soviet Union (17%), and Japan (14%).

### *b. Data processing*

Our overall aim in processing the data is to produce a gridded, monthly-mean climatology of the oxygen anomaly for the World Ocean of the highest possible quality. The data processing, detailed in the Appendix, is composed of five steps: (1) vertical interpolation of temperature, salinity and oxygen observations to standard depth levels; (2) computation of the oxygen anomaly at constant atmospheric pressure; (3) filtering of the oxygen anomaly to remove erroneous and unrepresentative data; (4) binning the oxygen anomaly onto a horizontal and monthly grid; and (5) objective analysis (horizontal interpolation and smoothing) of the oxygen anomaly in order to fill in data-void areas and

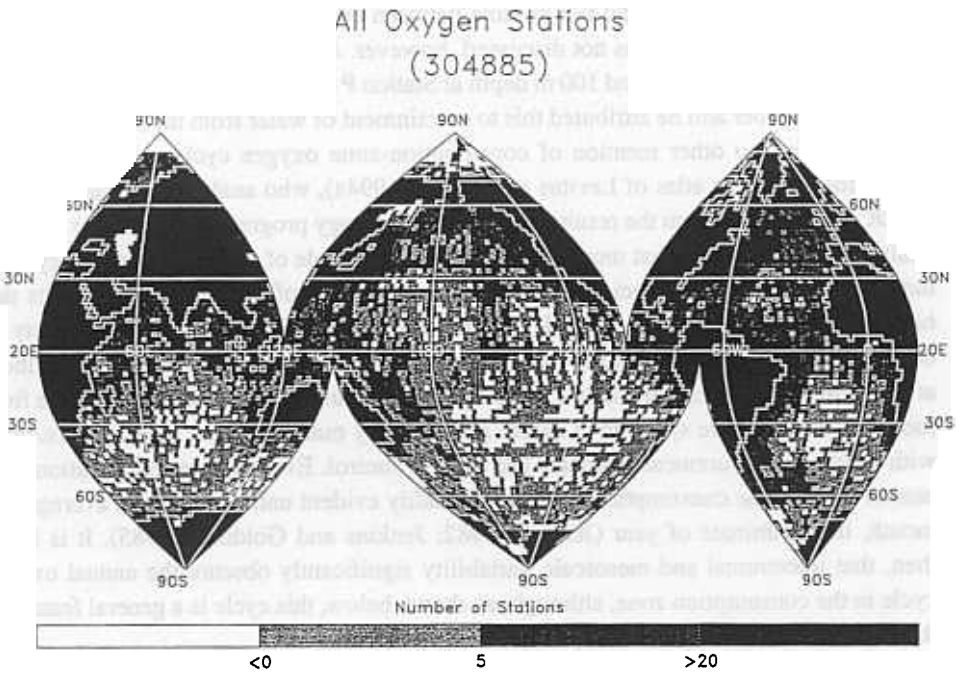


Figure 2. Distribution of stations containing oxygen in the March 1994 NODC Station Data Archives. The grid is nearly equal-area, with grid boxes approximately 220 km by 220 km (see Appendix) and is plotted on an interrupted sinusoidal projection, also equal-area.

to minimize the impact of nonseasonal variability. From the final surface maps, a second set of surface maps was produced that take into account climatological variations in sea level pressure, as detailed in the Appendix.

*c. Impact of data sparsity*

The reliability of the objectively-analyzed fields of the oxygen anomaly is limited by sparseness of coverage, interannual variability and measurement error. To assess the combined impact of data sparseness and interannual variability, we applied steps 4 and 5 above to temperature observations with exactly the same temporal and spatial resolution as the oxygen anomaly. The resulting maps were then averaged over 12° latitude bands and an annual harmonic was fit to these averages. The amplitudes of these fits are shown in Figure 3 with the amplitudes computed from the atlas of Shea *et al.* (1992) in the same way. The atlas of Shea *et al.* (1992) is not likely to suffer significantly from data sparsity because it is based on over 1.5 million observations, more than five times the number of observations in our reduced data set of temperature. Due to the difference in coverage between the two data sets, the amplitudes computed from the reduced data set are generally less than those computed from the larger data set. In the Northern Hemisphere, however, the differences are relatively small. For example, in the zone between 30N and 42N, the

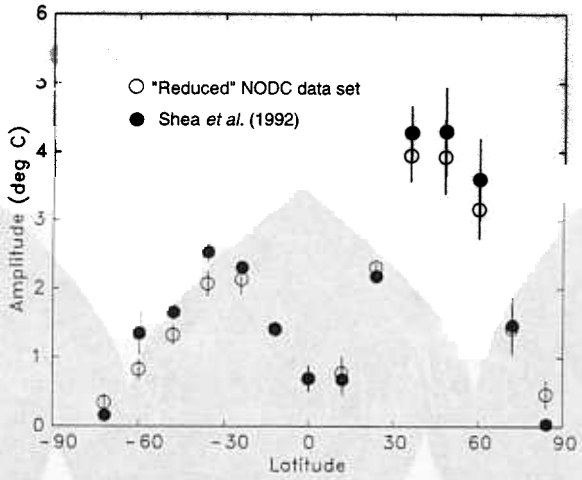


Figure 3. Amplitude of the annual harmonic of sea surface temperature as a function of latitude for two different data sets: (1) the atlas of Shea *et al.* (1992) (filled circles) and (2) objective analyses of temperature data from the NODC archives that have exactly the same temporal and spatial resolution as the oxygen anomaly in this study (open circles). For both data sets, monthly maps were averaged over 12° latitude bands before fitting the annual harmonic. The error is the standard deviation of the fit.

amplitude from the reduced data set is only 8% smaller than the amplitude from the larger data set. The differences in the Southern Hemisphere are greater, reflecting the relative paucity of data in the reduced data set (Fig. 2): the difference is 19% between 30S and 42S, and 39% between 54S and 66S. A similar comparison of amplitudes in individual ocean basins from the Southern Hemisphere (not shown), reveals that the difference in amplitudes is largest in the South Pacific and smallest in the South Atlantic. Again, these differences reflect the data distribution (Fig. 2). At polar latitudes the reduced data set yields a larger amplitude because the sea surface temperature under sea ice is considered to be constant in the Shea *et al.* (1992) atlas. These results suggest that data sparsity has not severely limited our ability to resolve the annual cycle of the oxygen anomaly (at least in the zonal mean sense) outside of the Southern Ocean. This analysis also provides a rough estimate of how much lower the amplitudes of the oxygen anomaly in the climatology are with respect to the true amplitudes.

## 4. Horizontal distributions

### *a. The sea surface*

The binned oxygen anomaly in surface waters for January and June (Fig. 4) shows the strong summertime bias of the data set and also the strong seasonal signal in the oxygen anomaly itself. The horizontal patterns of seasonal variability at the sea surface can be seen more clearly in the December–January and June–July averages of the objectively analyzed

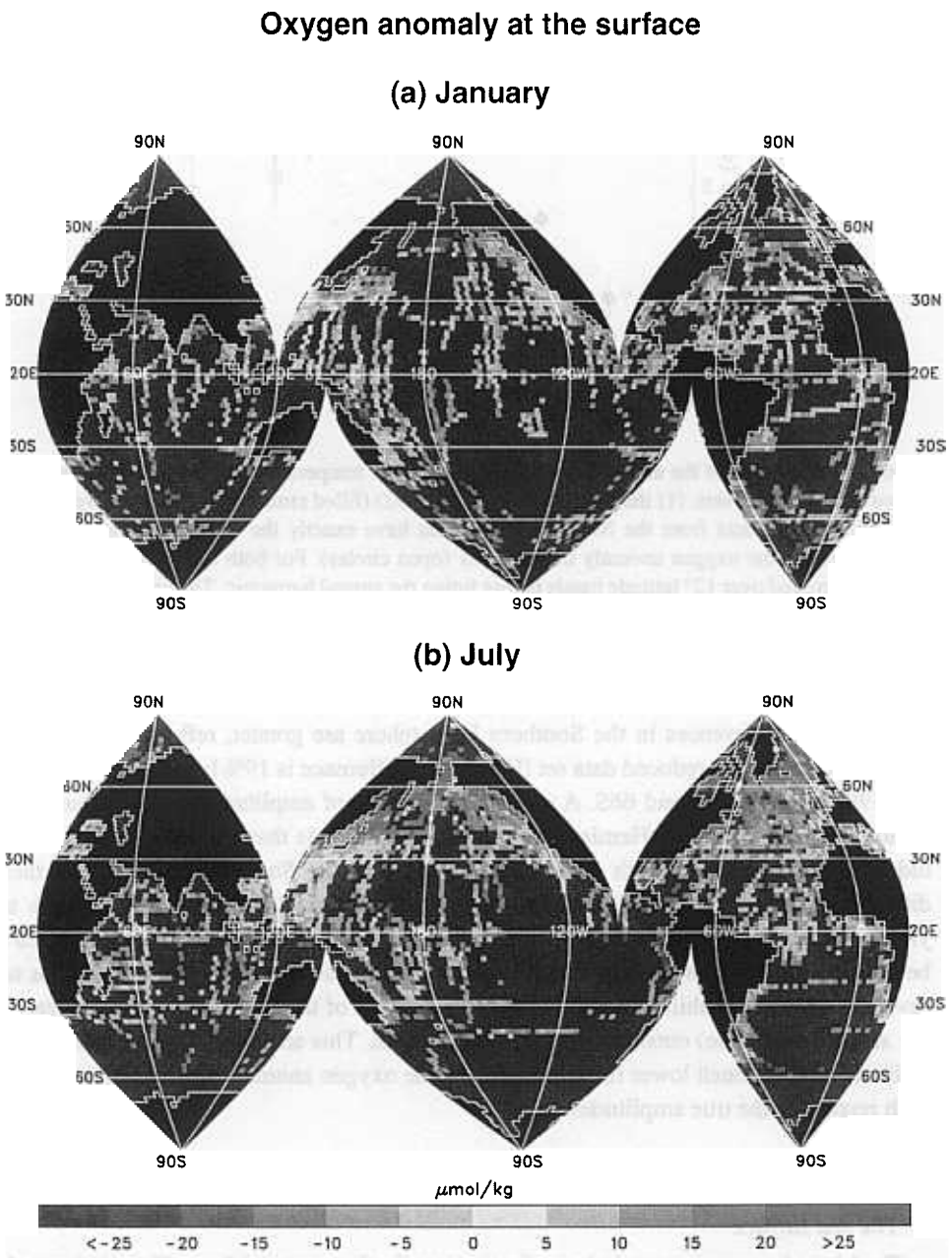


Figure 4. The oxygen anomaly in surface waters binned into the equal-area grid for (a) January and (b) July. The oxygen anomaly was computed at a total pressure of one atmosphere.

fields (Fig. 5). Overall, the annual cycle in surface waters is consistent with the canonical surface cycle discussed earlier.

*i. The Northern Hemisphere.* Surface waters of the North Atlantic and North Pacific show an annual cycle that is especially pronounced in the higher latitudes (Fig. 5). During early winter, surface waters are undersaturated everywhere northward of about 40N in the Pacific and 30N in the Atlantic, and are mildly supersaturated to the south (Fig. 5a). The regions of greatest undersaturation in the Northern Hemisphere are the Bering Sea, the Labrador Sea/Baffin Bay region and the North Sea. In general, undersaturation tends to be relatively high in the western portions of the North Atlantic and North Pacific. During the early summer in the North Atlantic and Pacific, waters are almost everywhere supersaturated, and particularly high values of the oxygen anomaly are reached in the Greenland and Norwegian Seas, the Labrador Sea/Baffin Bay region, the Sea of Okhotsk and the Gulf of Alaska (Fig. 5b). On the whole, oxygen supersaturation is relatively high in the western portions of the North Atlantic and North Pacific, particularly poleward of 30N. Thus, it is clear that the amplitude of the annual cycle increases toward the west in the North Atlantic and North Pacific, particularly at middle and high latitudes. This is not surprising, since the annual cycles in sea-surface temperature and mixed layer depth—which drive the thermal and biological components of the annual oxygen cycle—are stronger in the west (e.g., see the atlas of Levitus [1982]).

The early summer and early winter maps of Figure 5 do not capture seasonal variations in the surface waters of the North Indian Ocean because the semiannual cycle is strong there, due to monsoon forcing. We put off our discussion of the North Indian Ocean to a later section (5c).

*ii. The Southern Hemisphere.* The Southern Hemisphere also has an annual cycle that increases in amplitude with latitude, but surface waters far south are permanently and deeply undersaturated. Permanent undersaturation can occur for two reasons: heat flux from the ocean to the atmosphere or relatively low new production in the face of an upward flux of water depleted in oxygen by respiration (Keeling *et al.,* 1993). Both of these processes occur in the polar regions of the Southern Ocean, the latter consistent with the high nutrient concentrations, high rates of upwelling and deep mixed layers in this region. The equatorward extent of undersaturation during the winter (Fig. 5b) is similar to that in the Northern Hemisphere. During the summer, surface waters become only mildly supersaturated, with the greatest supersaturation occurring in a band between about 40S and 50S (Fig. 5a).

*iii. The tropics.* Outside of the Eastern Equatorial Pacific, there is little seasonal variability of the surface oxygen anomaly in the tropics. The greater undersaturation during June–July compared with December–January in the Eastern Equatorial Pacific (Fig. 5) is broadly consistent with the annual cycle in sea surface temperature induced by upwelling and the

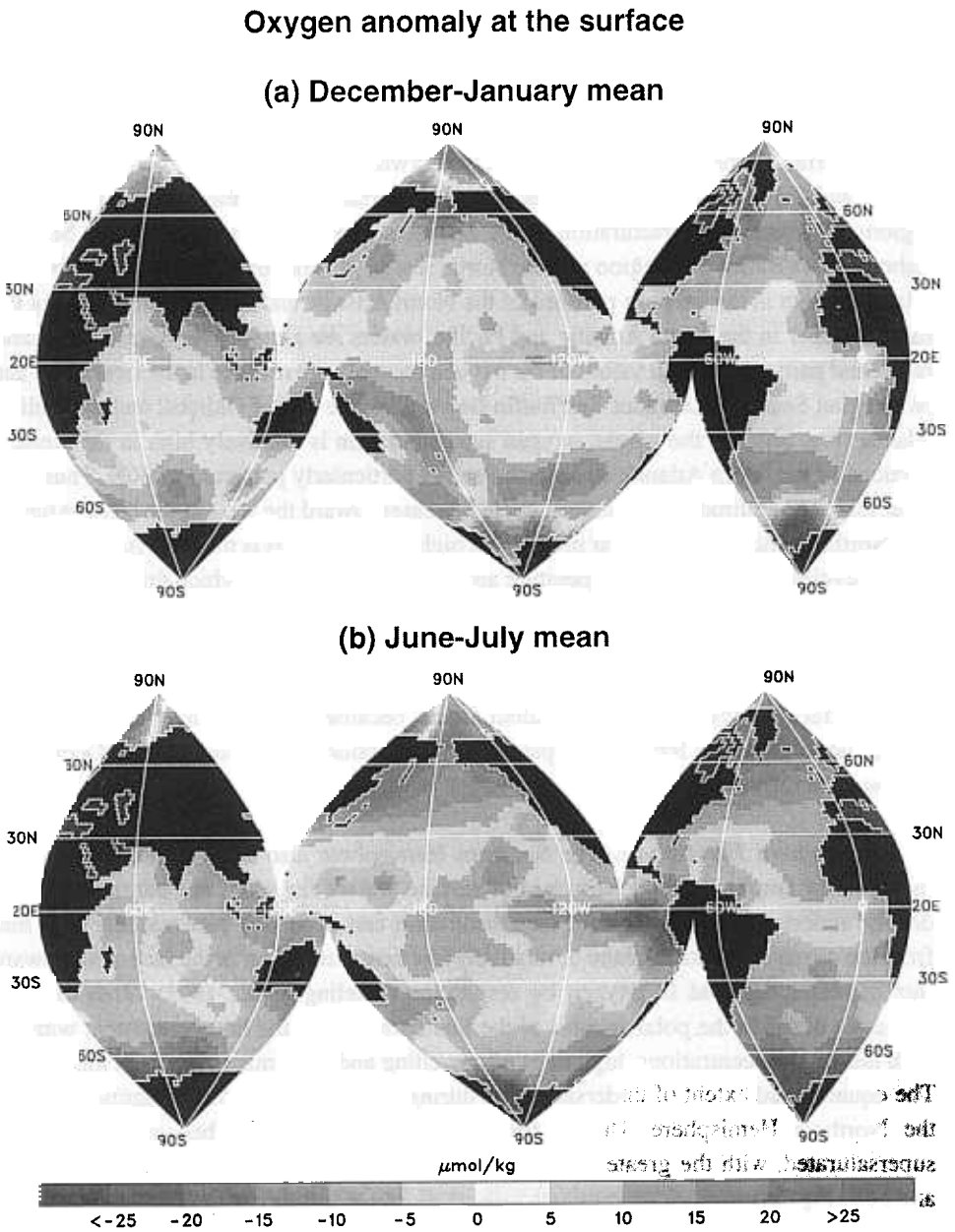


Figure 5. The objectively-analyzed oxygen anomaly in surface waters: (a) December–January and (b) June–July averages. These analyses were adjusted to account for climatological sea level pressure variations, as described in the Appendix.

depth of the thermocline according to Wyrtki (1981): the cold tongue is strongest between August and October and weakest between February and March. A second zone of undersaturation in the tropics is found in the Australasian Mediterranean Seas. We know of no mention of this feature in the literature, though it can be seen in the atlases of Levitus (1982) and Levitus and Boyer (1994a). This is a region of moderate upwelling (Wyrtki, 1961, page 139; Tomczak and Godfrey, 1994, page 43; Shaw *et al.*, 1996), but also one believed to have high vertical mixing due to topographic effects (Gordon, 1986). We would therefore expect surface nutrients and primary productivity to be higher in this region than in surrounding waters. This is indeed the case, as can be seen in the nutrient atlas of Conkright *et al.* (1994) and in many primary productivity atlases (Berger *et al.*, 1987; Antoine *et al.*, 1996). We suspect, therefore, that the undersaturation in the surface waters of the Australasian Mediterranean Seas is due to the upward transport (by advection and mixing) of oxygen-depleted water.

*b. The shallow consumption zone*

To illustrate the horizontal patterns of seasonal variability in the shallow consumption zone, we subtracted the September–October average from the March–April average at 125 m (Fig. 6). Almost everywhere poleward of 30° latitude the oxygen anomaly at 125 m is greater in the early spring than in the early fall, a cycle consistent with the canonical consumption zone cycles discussed earlier. As in surface waters, the amplitude at 125 m increases toward the west in the North Atlantic and North Pacific (Fig. 6), consistent with the strong seasonality in ventilation and production in the west. We suspect that the large spatial variability in the tropics is the result of aliasing interannual and mesoscale variations. The tropics are particularly susceptible to this phenomenon because the vertical oxygen gradients are large; small vertical displacements of the thermocline can produce large variations in the oxygen anomaly. It may be possible to eliminate this variability by analyzing the oxygen anomaly on isopycnal surfaces instead of constant-depth surfaces.

## 5. Harmonic analysis

In order to reveal most clearly the vertical and latitudinal trends in the phase and amplitude of the annual cycle, we averaged the objectively-analyzed fields across 12° latitude bands for each ocean. A total of 34 zones were created: 14 in the Atlantic Ocean (78S to 90N), 12 in the Pacific Ocean (78S to 66N), and 8 in the Indian Ocean (66S to 30N). The resulting time-series for each zone was fitted with an annual harmonic at each standard depth:

$$A \cos\left(\frac{2\pi}{12 \text{ months}}(t - t_o)\right), \tag{1}$$

where $A$ is the amplitude (μmol kg$^{-1}$), $t$ is the time since the beginning of the year (months) and $t_o$ is the phase (months)—the time at which the fit is a maximum. Figure 7 shows an

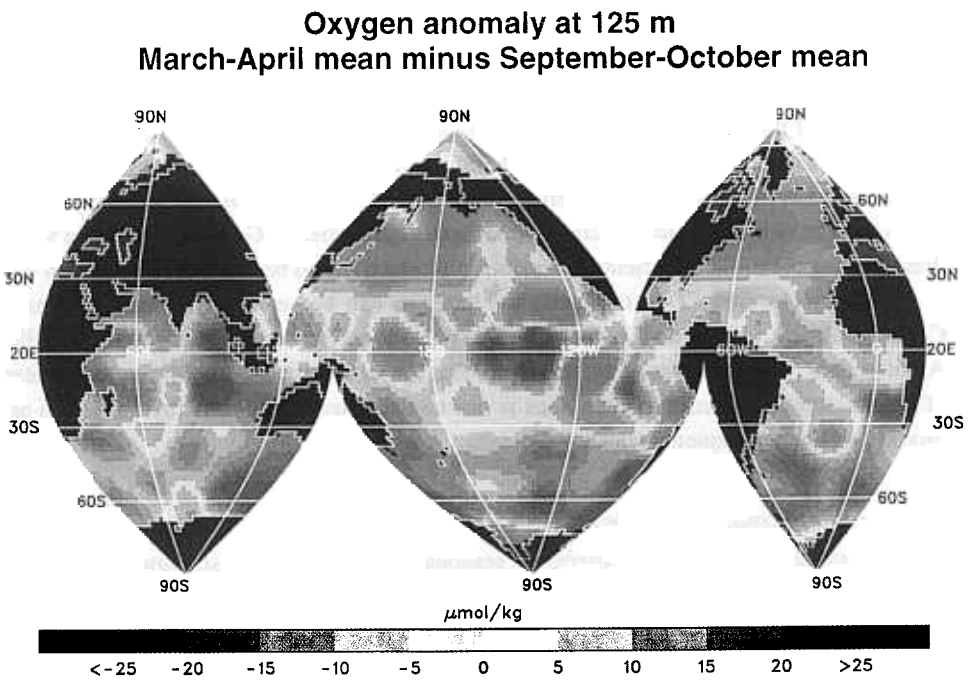


Figure 6. March–April average minus September–October average of the objectively-analyzed oxygen anomaly at 125 m.

example from the latitude band between 30N and 42N in the Pacific Ocean. A single harmonic represents each of the cycles well, and the production and consumption zone cycles are consonant with the canonical cycle discussed earlier.

In the following, we consider the tropics to be 18S to 18N, middle latitudes to be 18° to 54° latitude, and high latitudes to be 54° to 90° latitude. We describe the phasing of the cycles in terms of the month when the fit to the annual cycle reaches a maximum; this may not always be the same as the month when the oxygen anomaly itself is highest. In order to maintain consistency with deeper levels, the surface maps were not pressure-corrected before making the fits.

*a. The middle and high latitudes of the Atlantic, Pacific and South Indian Oceans*

The middle and high latitudes of the Atlantic, Pacific and South Indian Oceans (Figs. 8 to 12) show a number of similar features, and are therefore discussed together. Because the North Indian Ocean is dominated by the monsoon and has a distinctly different character from the other oceans, it will be discussed separately.

*i. The production zone.* The oxygen anomaly in the surface waters of almost all of the zones of the middle latitudes of the Atlantic, Pacific and South Indian oceans reaches a maximum in early summer (Figs. 8 to 12), consistent with the time of rapid warming and high rate of

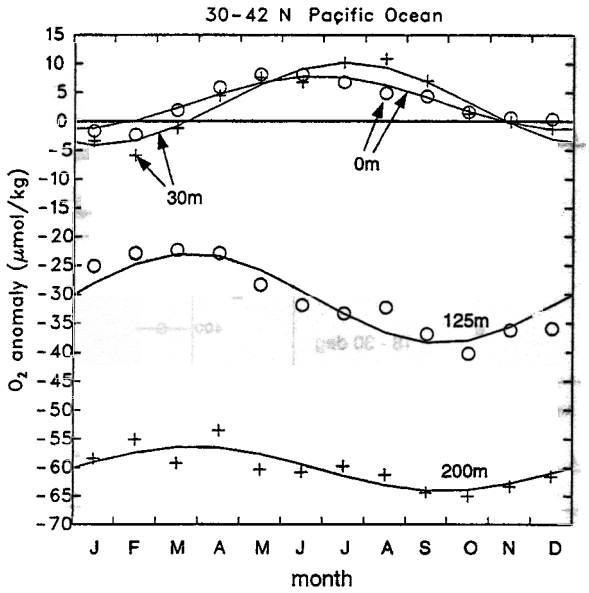


Figure 7. Time-series of the average oxygen anomaly (circles and crosses) at 0, 30, 125 and 200 m in the Pacific Ocean between 30N and 42N. The lines are least-squares, annual harmonic fits. The surface values have not been pressure-corrected.

new production. Exceptions are in the Pacific between 18N and 30N (maximum in late spring) and 18S to 30S (maximum in late summer). The corresponding minimum of the oxygen anomaly in early winter is consistent with the time of rapid cooling and entrainment of oxygen-depleted water from below the mixed layer. Higher latitudes generally lag lower latitudes by one or two months, with the zone between 54S and 66S in the Indian Ocean as the one exception. In high latitudes, the amplitude has a local maximum at or very near the surface and a phase that is constant in the upper 50 m or so, while in middle latitudes, the amplitude generally increases with depth, with deeper layers lagging the surface. The midlatitude pattern is consistent with the buildup of oxygen in the shallow oxygen maximum (Reid, 1962; Shulenberger and Reid, 1981).

*ii. The compensation depth.* At a characteristic depth that varies between about 30 and 130 m in middle and high latitudes, the amplitude of the annual cycle generally reaches a minimum simultaneous with an abrupt phase shift (Figs. 8 to 12). Because this feature is ubiquitous, we have given it a name: the *oxygen nodal depth.* The nodal depth has two important features in middle and high latitudes: (1) the annual cycle just below the nodal depth generally lags the annual cycle just above the nodal depth by a few months; and (2) the nodal depth decreases toward the poles.

In the context of the canonical cycles presented in Figure 1, an abrupt phase shift is an expected consequence of the separation of the realms of net photosynthesis and net

North Atlantic

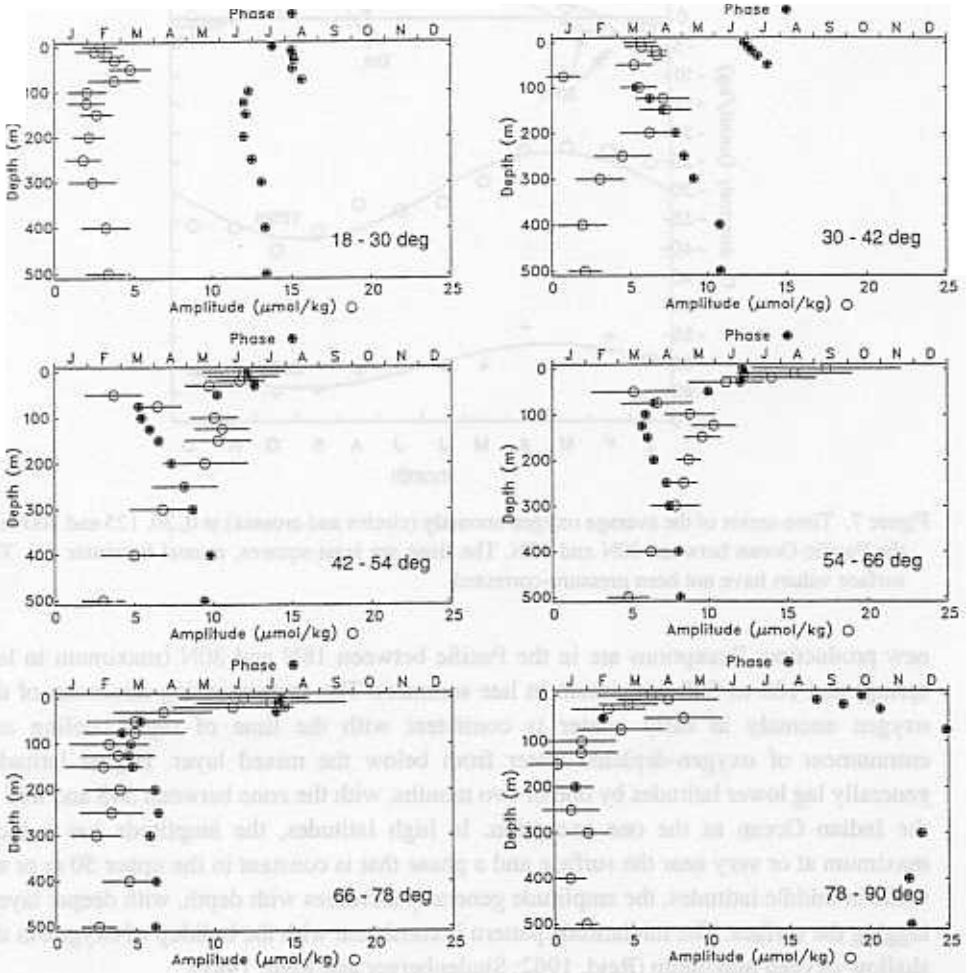


Figure 8. Amplitude (open circles) and phase (filled circles) of the annual cycle of the average oxygen anomaly in 12° latitude bands of the middle and high latitudes (poleward of 18° latitude) of the North Atlantic Ocean as a function of depth. Error bars on the amplitude are ±1 standard deviation of the annual harmonic fit. The phase is only plotted if the amplitude is significantly different from zero. Surface values were not corrected for pressure variations.

respiration at the compensation depth. In the spring and summer, when the compensation depth lies within the seasonal thermocline, oxygen accumulates above the compensation depth and decreases below the compensation depth. In the fall and winter, when the mixed layer depth becomes greater than the compensation depth, both the $\Delta[O_2]$ increase above and the $\Delta[O_2]$ decrease below the compensation depth will tend to be erased by vertical

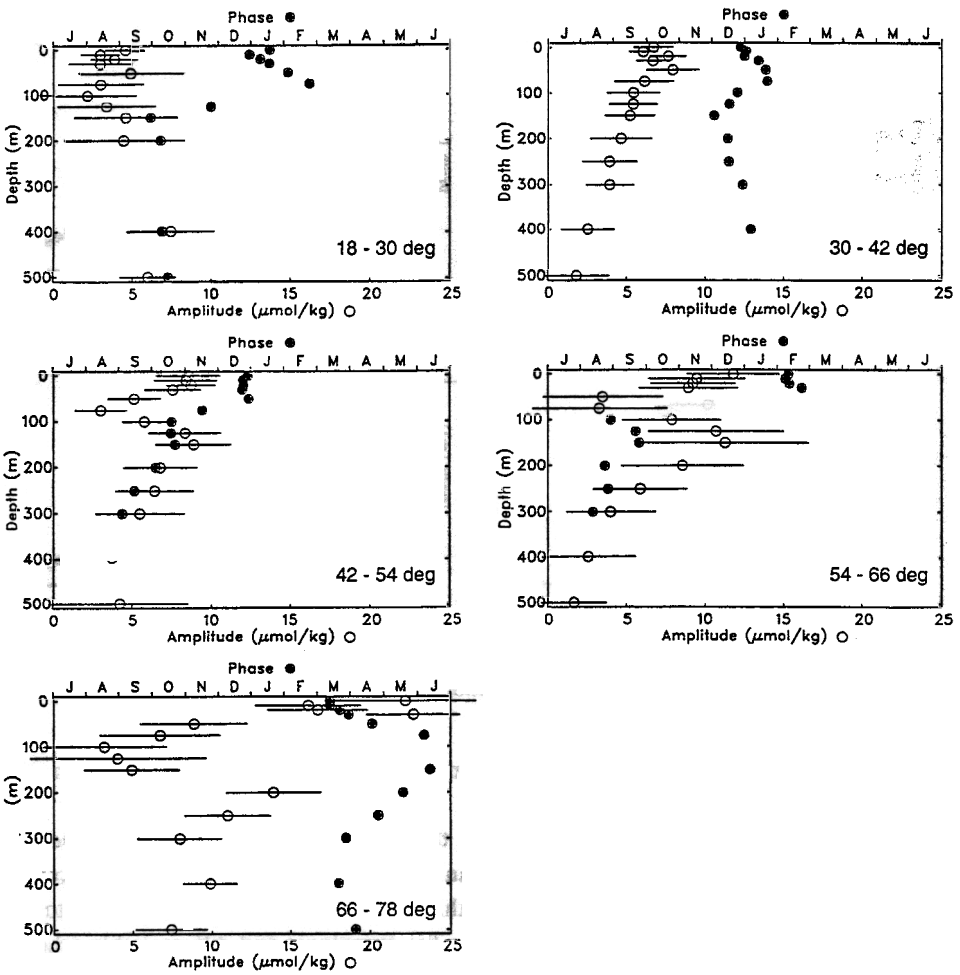


Figure 9. Amplitude and phase of the annual cycle in the middle and high latitudes of the South Atlantic Ocean. Note that the axis for the phase has been shifted six months with respect to the Northern Hemisphere. See caption of Figure 8 for more details.

mixing. From this perspective we expect that there should be a close correspondence between the observed nodal depth and actual spring- or summertime compensation depth. This interpretation provides an explanation for the observed trend in the nodal depth with latitude. One expects the compensation depth to decrease towards the poles because the compensation depth is thought to increase with the penetration of light (Richards, 1957). The latter decreases polewards because of the poleward decrease in solar radiation and the

North Pacific

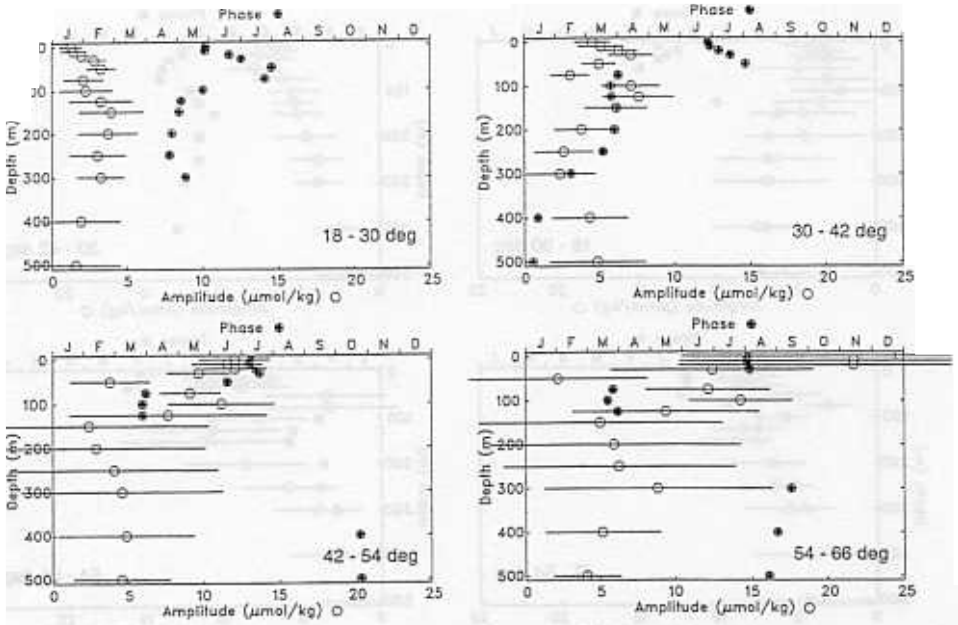


Figure 10. Amplitude and phase of the annual cycle of the oxygen anomaly in the middle and high latitudes of the North Pacific Ocean. See caption of Figure 8 for details.

increase in the opacity of seawater (as determined by the chlorophyll content) from middle to high latitudes (Yoder *et al.*, 1993).

We developed an algorithm to determine the oxygen nodal depth based on the abrupt change in phase with depth. (The minimum in the amplitude is not always well resolved, so it was not used to determine the nodal depth.) First, the phase was interpolated to a grid with a vertical resolution of one meter using the monotonic and differentiable scheme of Steffen (1990). Only those points where the amplitude is significantly different from zero were used (determined from the standard error of the fit), since the phase is otherwise not well defined. The nodal depth was determined to be the depth at which the absolute value of the first derivative of the phase with respect to depth ($\partial t_o/\partial z$) is a maximum.

Direct estimates of the compensation depth (based on bottle incubations of the plankton community) in open ocean water are few. Clarke (1936) found the compensation depth to be around 100 m in the Sargasso Sea during summer. Langdon *et al.* (1995) found values less than 15 m in the Subarctic Atlantic during spring and summer. The compensation depth has more commonly been estimated indirectly from the light field (often model-based) and the compensation light intensity (Sverdrup, 1953), the amount of light at which respiration is equal to photosynthesis. For our purposes, respiration must include all

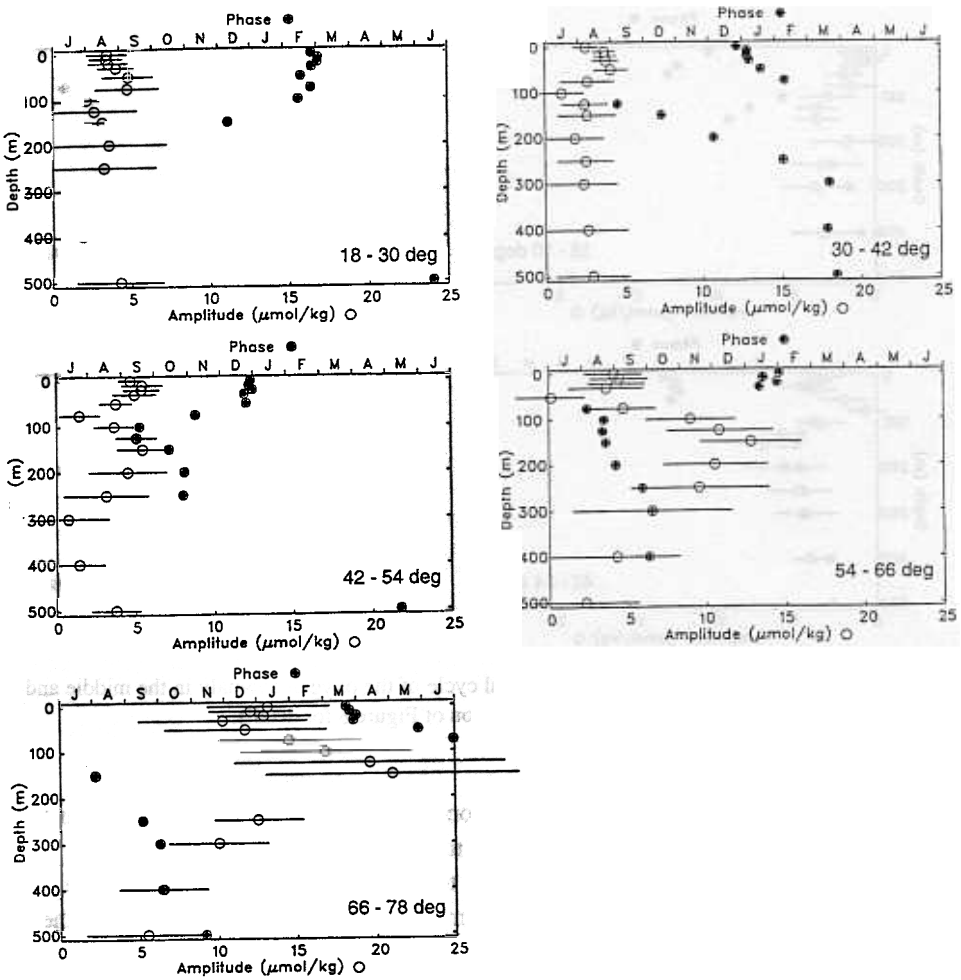


Figure 11. Amplitude and phase of the annual cycle of the oxygen anomaly in the middle and high latitudes of the South Pacific Ocean. See caption of Figure 8 for details.

biogenic sinks of oxygen: phytoplankton respiration, zooplankton grazing, and bacterial activity. There are an abundance of estimates of the compensation light intensity based on phytoplankton respiration alone, and they vary widely. Parsons *et al.* (1984) gave a range of 1 to 6 W $m^{-2}$ (4 to 25 $\mu E\ m^{-2}\ s^{-1}$),[3] though there are a considerable number of estimates outside of this range (Raymont, 1980). Platt *et al.* (1991) reviewed other forms of

3. For blue-green water with pigment concentrations between 0.1 and 1.0 mg $m^{-3}$, Morel and Smith (1982) show that 1 W $m^{-2}$ is equivalent to 4.17 $\mu E\ m^{-2}s^{-1}$ ($E$ = Einstein = photon).

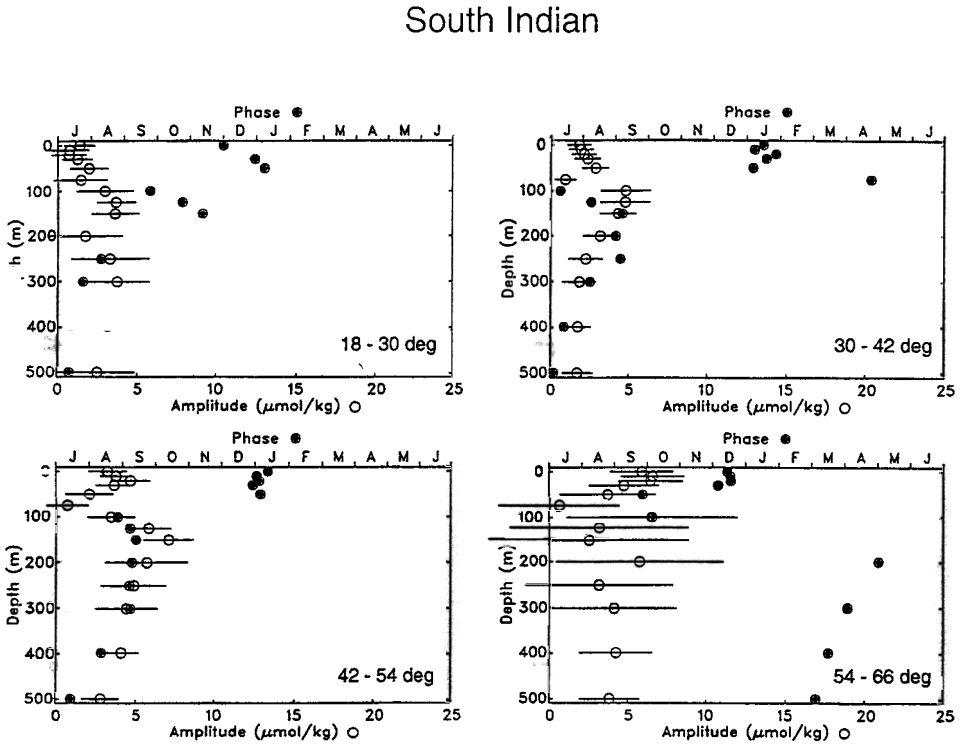


Figure 12. Amplitude and phase of the annual cycle of the oxygen anomaly in the middle and high latitudes of the South Indian Ocean. See caption of Figure 8 for details.

respiration and estimated that phytoplankton respiration is somewhat more than half of total respiration, while zooplankton grazing makes up most of the balance.

We assumed the nodal depth to be equal to the summertime compensation depth, and determined the compensation light intensity most consistent with our estimates of the nodal depth. We started by relating the summertime compensation depth ($z_c$) to the mean compensation light intensity ($I_c$) for each zone (12° latitude band) using

$$I_c = rI_o \exp(-kz_c), \tag{2}$$

where $I_o$ is the mean surface solar radiation for each zone during the middle of summer (August in the Northern Hemisphere and February in the Southern Hemisphere), $r$ is the fraction of surface solar radiation that is photosynthetically-active radiation (PAR), and $k$ is the mean diffuse attenuation coefficient for PAR for each zone during the middle of summer. The attenuation of light is significantly affected by the chlorophyll concentration; to include this effect, the formulation of $k$ by Morel (1988) was used:

$$k = 0.121[\mathrm{Chl}]^{0.428}\mathrm{m}^{-1}, \tag{3}$$

where [Chl] is the chlorophyll concentration in mg $m^{-3}$ averaged over the euphotic zone. Modeling the attenuation of PAR with a single exponential is a simplification (Morel, 1988), but given the uncertainties in many of the model inputs (e.g., solar radiation and chlorophyll concentration), we believe that a more elaborate model is unjustified.

The chlorophyll concentrations were taken from the satellite-based climatology of Yoder *et al.* (1993). Satellite estimates of chlorophyll are effectively averaged over one extinction depth, so these values should be reasonably representative of the euphotic zone as a whole. Yoder *et al.* (1993) computed the average chlorophyll concentration for each month in several zones (larger than ours) and we simply chose the appropriate summertime value for each of our zones from the figures in their paper. Solar radiation data were taken from the climatology of Oberhuber (1988), and a value of 0.45 was used for $r$ (Baker and Frouin, 1987).

The results of this calculation show that the light-based estimates of the compensation depth most closely correspond to the oxygen nodal depth when $I_c = 1$ W $m^{-2}$ (4 $\mu E\, m^{-2}\, s^{-1}$), the lower end of the range based on phytoplankton respiration alone (Fig. 13). Though this value is somewhat lower than expected, especially given the likely importance of other forms of respiration, it is encouraging that a reasonable value was obtained and that two disparate methods of estimating the compensation depth give similar latitudinal trends and interbasin differences. The oxygen nodal depth is greater in the South Atlantic and South Pacific than in the North Atlantic and North Pacific. The light-based estimates show similar differences (except in the Subtropical Pacific) due primarily to the greater chlorophyll concentrations in the Northern Hemisphere (Yoder *et al.*, 1993).

*iii. The consumption zone.* Just below the nodal depth (i.e., in the shallow consumption zone) the oxygen anomaly amplitude generally reaches a second local maximum; of the 24 zones considered in this section, 18 have the consumption-zone maximum between one and two hundred meters. In the shallow consumption zone, the maximum almost always occurs in winter or spring and mostly in late winter or early spring, consistent with a ventilation-respiration cycle (Worthington, 1959; Jenkins and Goldman, 1985). There is a tendency, particularly in the latitude bands poleward of 30°, for the maximum in the shallow consumption zone to occur earlier toward higher latitudes. This, combined with the increasing phase lag toward the poles in surface waters, makes the phase shift between the production and shallow consumption zones increase toward the poles.

Deeper in the consumption zone, the amplitude of the annual cycle decreases with depth throughout most of the consumption zone, consistent with the decrease in remineralization and ventilation with depth (Jenkins and Goldman, 1985) or in the seasonality of both processes. This pattern is clearest in the North Atlantic, but is present in all of the other basins, ignoring those amplitudes that are not significantly different from zero. There are some notable exceptions, limited to middle latitudes, where the amplitude increases with depth: 18S to 30S and 18N to 30N in the Atlantic, 30S to 42S in the Pacific, and 30N to 42N in the deeper (300 to 500 m) Pacific. We have no explanation for these trends.

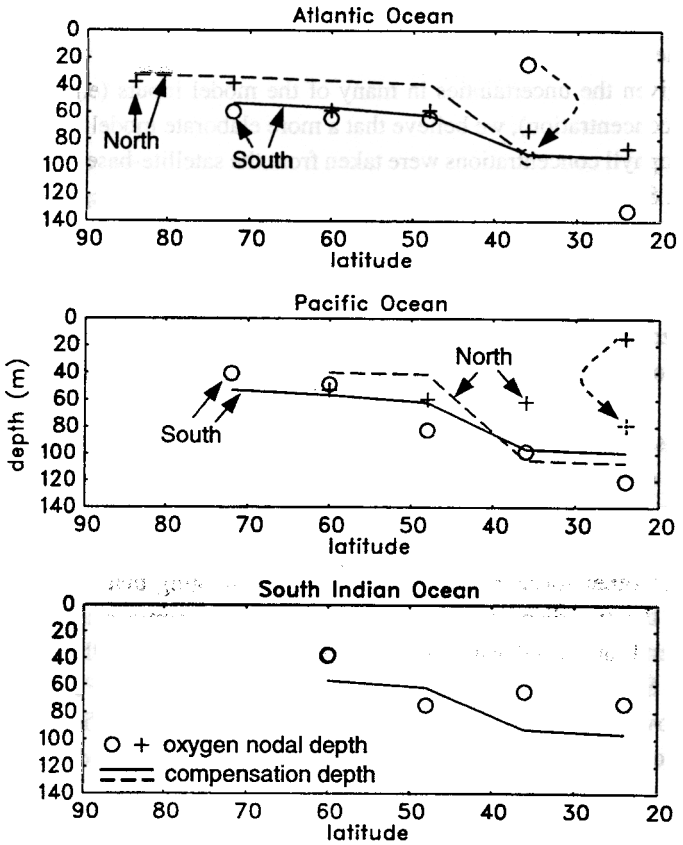


Figure 13. Oxygen nodal depth (symbols) and summertime compensation depth (lines) as a function of latitude. The latter is computed from a compensation light intensity of 1 W $m^{-2}$ (4 $\mu E$ $m^{-2}$ $s^{-1}$). See the text for details. North and south are plotted together to highlight inter-hemispheric differences. Symbols with dashed arrows pointing to them are our estimates of the oxygen nodal depth based on a visual inspection of the corresponding panels in Figures 9 and 10.

In the consumption zone, the maximum in the oxygen anomaly occurs later in the year with increasing depth. Again, the pattern is clearest in the North Atlantic (outside the Arctic) and is consistent with the trend at Station S (Jenkins and Goldman, 1985). Notable exceptions are seen south of 42S in the Atlantic, 30N to 42N in the deeper (200 to 500 m) Pacific, and throughout the middle and high latitudes of the South Indian Ocean.

*b. The Tropical Atlantic and Pacific Oceans*

Because seasonal forcing is generally weaker and interannual variability is greater in the tropics, annual cycles in this region are generally noisier (Figs. 14 and 15). Nevertheless, we find that a substantial portion of the water column in the tropics has significant annual cycles.

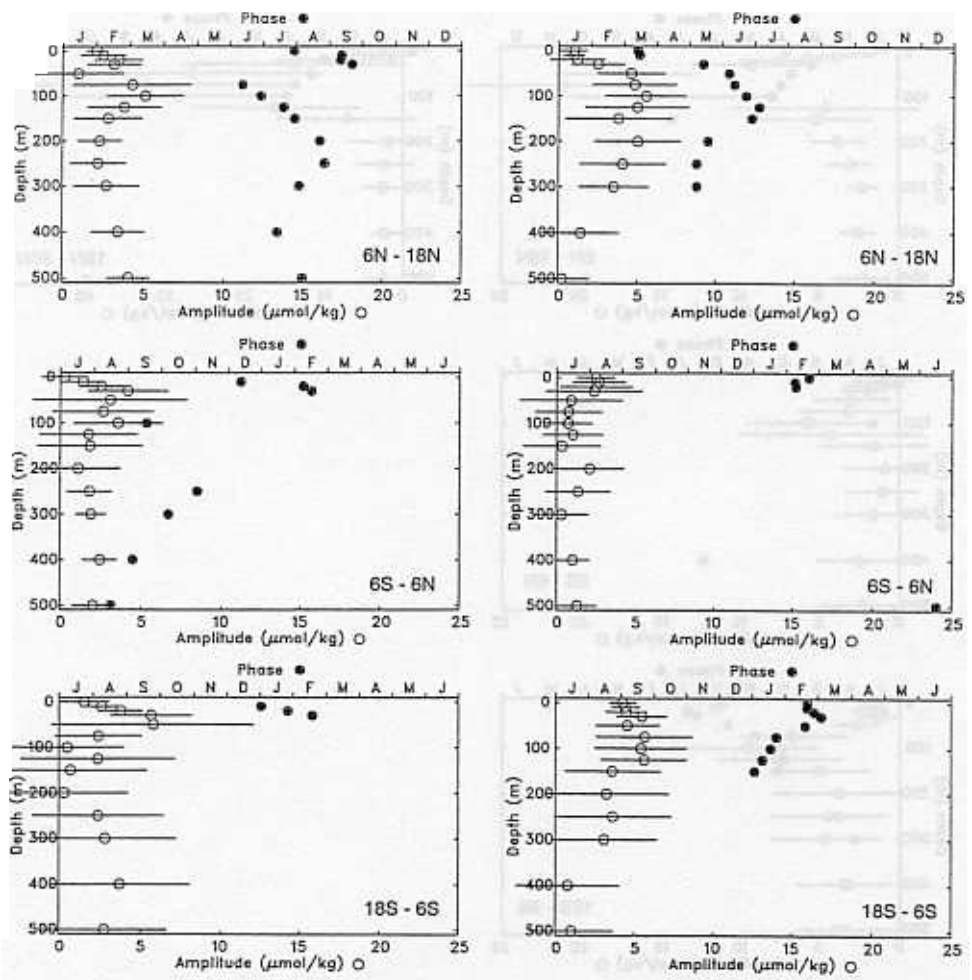


Figure 14. Amplitude and phase of the annual cycle of the oxygen anomaly in the Tropical Atlantic and Pacific Oceans. See caption of Figure 8 for details. Note that the axis for the phase of the latitude band between 6S and 6N is the same as that of the bands to the south.

*i. Surface waters (0 to 50 m).* In the surface and near-surface waters of the Tropical Atlantic (Fig. 14), we find barely statistically significant annual cycles, with the maximum occurring between July and September north of 6N and between December and February south of 6N. The phasing is the same as that further poleward (in particular, between 18° and 30° latitude) in each hemisphere with the equatorial band (6N to 6S) tracking the Southern Hemisphere. Because the thermal equator is in the Northern Hemisphere, on average, it is not surprising that the latitude band between 6S and 6N has a surface cycle in

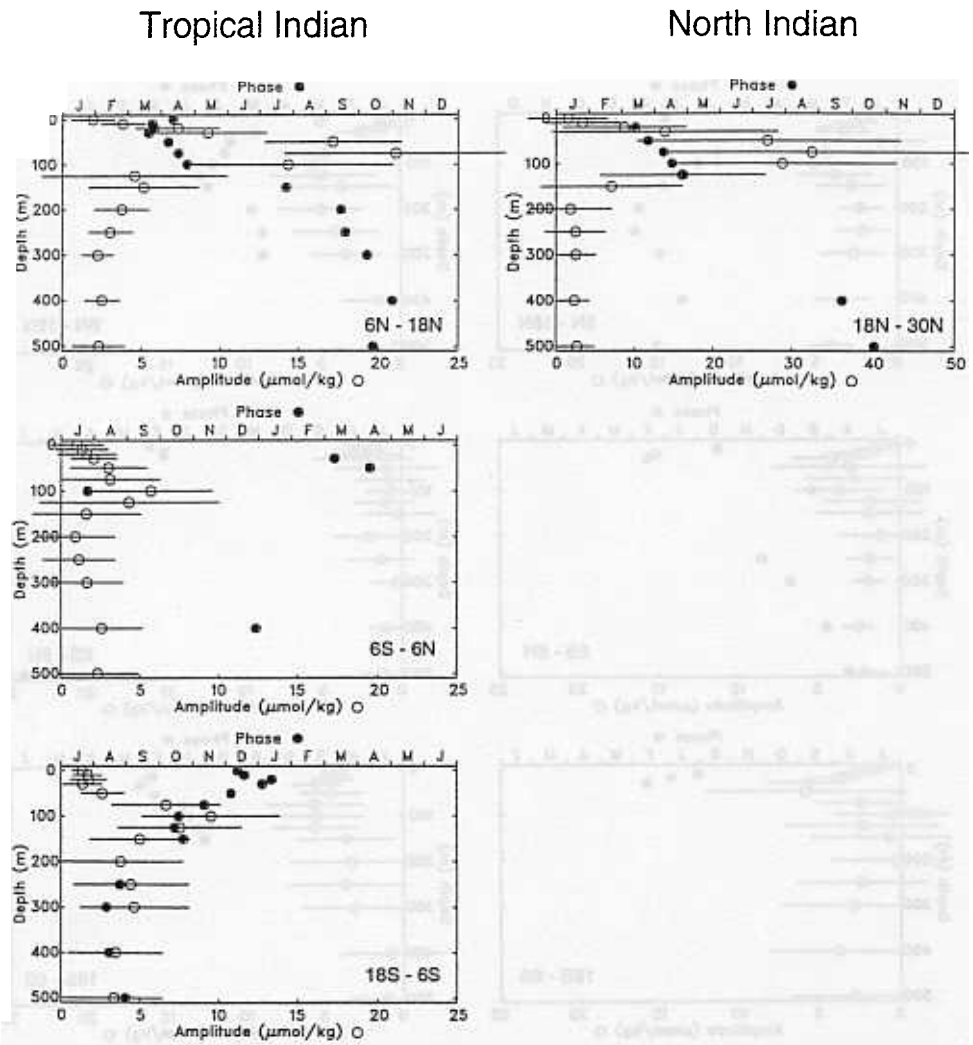


Figure 15. Amplitude and phase of the annual cycle of the oxygen anomaly in the Tropical and North Indian Ocean. See caption of Figure 8 for details. Note that the range of the horizontal scale for the North Indian Ocean is twice that of all other regions.

phase with the Southern Hemisphere cycles. In the upper 50 m, the phase and amplitude (where significant) increase with depth, again similar to the latitude bands farther poleward, and consistent with the seasonal accumulation of oxygen below the mixed layer.

The zonal mean cycles in surface waters of the Tropical Pacific (Fig. 14) are similar to those of the Tropical Atlantic except for the latitude band between 6N and 18N, where the phasing is unique in that the maximum occurs in late winter. Even though the equatorial zone (6S to 6N) in the Pacific tracks the Southern Hemisphere, the dominant cause of the

cycle in this zone may be different from that to the south. The upwelling signal in the Eastern Equatorial Pacific, discussed earlier, may dominate the zonal mean cycle.

*ii. Deeper waters (75–500 m).* We find well-resolved deeper cycles in the Pacific in the zones from 6S to 18S and from 6N to 18N, with both zones having maxima in late spring to early summer (Fig. 14). Deep, well-resolved cycles in the Tropical Atlantic are only found between 6N and 18N, and are similar to the corresponding cycles in the Pacific. We will show that these annual cycles are caused by vertical, adiabatic displacements of the thermocline. Such displacements are well-documented in the Tropical Atlantic and Pacific, and result from seasonal variations in surface winds (Meyers, 1979; Merle, 1983). Merle's (1983) analysis of the thermal structure of the Tropical Atlantic shows that the 20°C isotherm has a mean depth of about 100 m and is deepest in the early summer, on average, in the zone corresponding to our North Tropical Atlantic (6N to 18N). We find that the oxygen anomaly at 100 m in the North Tropical Atlantic peaks in the early summer, consistent with the motion of the thermocline. Along the equator, the 20°C isotherm has a mean depth of about 75 m, and the annual cycle is 180° out of phase between the East and West Atlantic (Merle, 1983). This may be why we do not find a significant amplitude of the zonal mean oxygen anomaly at 75 m in the Equatorial Atlantic. In the latitude band to the south, the annual cycle of the 20°C isotherm is similar to its northern counterpart, but we find no significant annual cycle in the oxygen anomaly, perhaps because the data density is lower in the south (Fig. 2).

A similar comparison may be made in the Pacific. Meyers's (1979) analysis shows that the 14°C isotherm between 6N and 18N has a mean depth of about 150 m and reaches its greatest depth in May. Consistent with this is our finding that the oxygen anomaly at this depth between 6N and 18N reaches its maximum value in June. As in the Equatorial Atlantic, we find no annual cycle in the zonal mean oxygen anomaly at depth in the Equatorial Pacific, presumably because of the zonal variability in the phase of the thermocline depth (Meyers, 1979). There is a weak annual cycle in the depth of the 14°C isotherm in the South Tropical Pacific (Meyers, 1979), but we find no significant annual cycles in the oxygen anomaly at the corresponding mean depth (~200 m), presumably because of the weakness of the signal or the paucity of data in this region (Fig. 2).

To determine whether the amplitude of the annual cycles in the oxygen anomaly are consistent with adiabatic displacements of the thermocline, we estimated the amplitude of the annual cycle of the oxygen anomaly caused by this process by using

$$A_{\Delta O_2} = A_T \left( \frac{\partial \overline{\Delta[O_2]}}{\partial z} \right) \left( \frac{\partial \overline{T}}{\partial z} \right)^{-1}, \tag{4}$$

where $z$ is the depth, $T$ is the temperature, $A_T$ is the amplitude of the annual temperature cycle and the overbar indicates an annual mean. We computed the terms on the right-hand side of (4) from the horizontal means of $\Delta[O_2]$ (from our climatology) and $T$ (from Levitus and Boyer [1994b]) within our 12° latitude bands. If the comparison between the observed

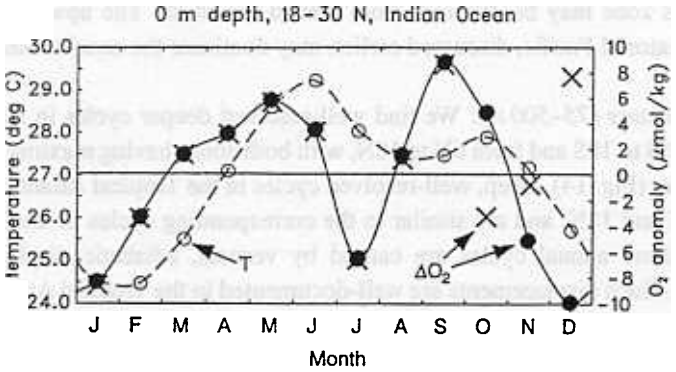


Figure 16. Average annual cycles of the temperature and oxygen anomaly in surface waters of the North Indian Ocean (18N to 30N). Filled circles represent $\Delta[O_2]$ from the unfiltered data set, and × indicates filtered $\Delta[O_2]$ data. The temperature data are from Levitus and Boyer (1994b).

and thermocline-induced $\Delta[O_2]$ amplitudes is restricted to where the phase difference between the observed annual cycles in $T$ and $\Delta[O_2]$ is less than three months, then, with very few exceptions, all of the significant amplitudes of the oxygen anomaly 75 m and deeper can be accounted for by the displacement of the thermocline. Thus, if there is a biological component to the annual cycle of the oxygen anomaly at depth in the tropics, its signal is overwhelmed by purely physical processes. It may be possible to extract the biological component by analyzing the oxygen anomaly on isopycnal surfaces.

### *c. The Tropical and North Indian Ocean*

*i. Surface waters.* From 6S to 18S in the Indian Ocean we find small annual cycles at the surface with fairly constant amplitude and phase from the surface to 50 m, with the maximum in the oxygen anomaly occurring in December or January (Fig. 15). These features are essentially the same as those in the latitude band between 18S and 30S.

In the latitude bands from 6S to 30N in the Indian Ocean, the amplitudes at the surface are generally very small or insignificant, and increase to 50 or 100 m depth, with the maximum in the oxygen anomaly occurring in March or April. The small amplitudes at the surface, particularly in the band between 18N and 30N, are due to the dominance of the semiannual cycle driven by the Asian monsoon. We show evidence of this in Figure 16, using both the filtered and unfiltered data. Surprisingly, the unfiltered data show a clearer semiannual signal than the filtered data. Possibly, our filtering scheme removed valid data during the months of October and December and retained erroneous (or unrepresentative) data. The unfiltered data set shows extrema in the oxygen anomaly that lead corresponding extrema in the temperature by about one month. In this sense, the surface oxygen cycle in the North Indian Ocean is consistent with the biological and physical processes considered in our earlier discussion of the canonical oxygen cycle in midlatitudes (Section 2).

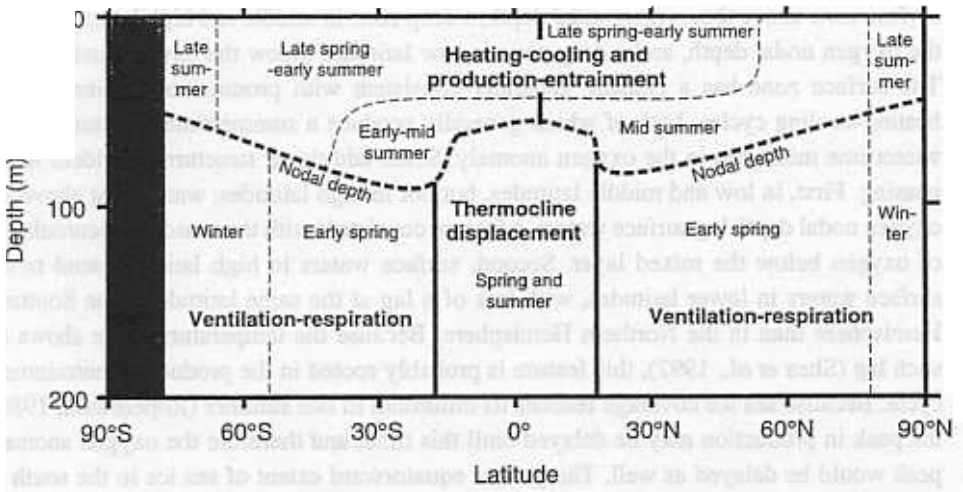


Figure 17. Schematic diagram showing the major features of the annual cycle of the zonal mean dissolved oxygen anomaly in the World Ocean, excepting the North Indian Ocean. Bold text indicates the major causes of the annual cycle. The seasons are locally defined and indicate the time when the oxygen anomaly is at a maximum. Waters near the equator are considered to be in the Southern Hemisphere.

*ii. Deeper waters.* The most pronounced features in the Tropical and North Indian Oceans are cycles in the depth range from 50 to 150 m north of 6N (Fig. 15). The largest amplitudes are found in the North Indian Ocean (18N to 30N) where they exceed 30 μmol $kg^{-1}$. The cycles are nearly as strong between 6N and 18N and marginally significant cycles are present between 6S and 6N. Between 6N and 30N, there is a clear phase lag with depth. A cycle with the opposite phase is found between 6S and 18S, where the amplitude reaches 10 μmol $kg^{-1}$. As in the Tropical Atlantic and Pacific, the subsurface oxygen cycles in the Tropical and North Indian Ocean are qualitatively consistent with adiabatic displacements of the thermocline. For example, Kumar and Unnikrishnan (1995) find the largest annual cycles in temperature at 100 m in the Bay of Bengal to reach their maximum values in May, similar to when we see the oxygen anomaly at 100 m peak in the two most northerly latitude bands in the Indian Ocean. As in the other ocean basins, these subsurface tropical temperature cycles can be explained from the seasonal variations in surface winds (Kumar and Unnikrishnan, 1995; Reverdin, 1987). From an analysis identical to that used for the Tropical Atlantic and Pacific Oceans (Eq. 4), we find that we can account for nearly all of the significant amplitudes in the North and Tropical Indian Ocean from adiabatic displacements of the thermocline.

## 6. Discussion and summary

Figure 17 summarizes in schematic form some of our findings about the annual cycle of the dissolved oxygen anomaly in the World Ocean. Three distinct zones are noted: a

surface zone above the oxygen nodal depth, a deep zone in middle and high latitudes below the oxygen nodal depth, and a deep zone in low latitudes below the oxygen nodal depth. The surface zone has a phasing generally consistent with production-entrainment and heating-cooling cycles, both of which generally produce a summertime maximum and a wintertime minimum in the oxygen anomaly. Some additional structure is evident in the phasing. First, in low and middle latitudes, but not in high latitudes, waters just above the oxygen nodal depth lag surface waters, a feature consistent with the seasonal accumulation of oxygen below the mixed layer. Second, surface waters in high latitudes tend to lag surface waters in lower latitudes, with less of a lag at the same latitude in the Southern Hemisphere than in the Northern Hemisphere. Because the temperature cycle shows no such lag (Shea *et al.,* 1992), this feature is probably rooted in the production-entrainment cycle. Because sea ice coverage reaches its minimum in late summer (Ropelewski, 1989), the peak in production may be delayed until this time, and therefore the oxygen anomaly peak would be delayed as well. The greater equatorward extent of sea ice in the south as compared to the north (Ropelewski, 1989) may explain why there is a north-south asymmetry in the lag.

Below the oxygen nodal depth in middle and high latitudes, the annual cycle of the oxygen anomaly is characterized by a spring maximum and a fall minimum, consistent with a ventilation-respiration cycle. Contributing to this cycle may be the seasonality in respiration. In other words, even without any annual cycle in ventilation, the annual cycle in respiration—likely a summer maximum and a winter minimum—would cause an annual cycle roughly in phase with the ventilation-respiration cycle. Further poleward, the maximum occurs a month or two earlier. We do not have an explanation for this feature, though we speculate that sea ice may be a factor, because the north-south asymmetry is similar to the surface cycles.

In low latitudes below the oxygen nodal depth, we find that adiabatic displacements of the thermocline are primarily responsible for the annual cycles in the dissolved oxygen anomaly. Even though the zonal mean oxygen anomaly below the nodal depth in tropical waters generally peaks in spring and in summer, we expect, from consideration of the thermal cycles (Merle, 1983; Meyers, 1979), that there is significant zonal variability in the phasing, particularly along the equator. We note that while adiabatic displacements of the thermocline occur poleward of 18° in the Atlantic and Pacific (Merle, 1983; Meyers, 1975; White, 1978), we find that their effect on the annual cycles in the oxygen anomaly is small.

The boundaries between the three zones in Figure 17 merit some comment. The two surface zones meet at around 5N, a boundary found in many climatological atmospheric and oceanic variables. This boundary represents the thermal equator, with the northward shift ultimately due to the greater land area in the Northern Hemisphere. The oxygen nodal depth, which separates the surface and deep zones in Figure 17, decreases from middle to high latitudes and is greater at a given latitude in the Southern Hemisphere than in the Northern Hemisphere. Both of these trends are consistent with an interpretation of the oxygen nodal depth as the summertime compensation depth. This interpretation breaks

down in the tropics, however, where the nodal depth is shallower but the compensation depth is deeper than in middle latitudes. In low latitudes, the relative strength of biological-thermal surface cycles and cycles caused by thermocline displacements determine the position of the nodal depth. The boundaries between the two deep regimes (at around 20N and 20S) are determined primarily by physical processes. Essentially, this boundary lies near the boundary separating adiabatic thermal cycles in the tropics from nonadiabatic thermal cycles in the middle latitudes.

A few important findings of our study are not included in Figure 17. The cycles in the North Indian Ocean are strikingly different from those in other oceans. First, a strong semiannual cycle in the oxygen anomaly has been found in surface waters consistent with annual cycles in other regions in that the oxygen anomaly leads temperature. Second, there are very large annual cycles in subsurface waters of the North Indian Ocean that are driven by displacements of the thermocline; these cycles are much larger than those found in other oceans at the same latitudes. Third, in the North Atlantic and North Pacific Oceans, the annual cycles above and below the oxygen nodal depth are much stronger in the west than in the east, consistent with the similar east-west asymmetry in physical forcing.

As this work is primarily descriptive, we make only modest efforts to delineate the relative importance of biological and physical causes of the annual cycles of the dissolved oxygen anomaly. For example, we do not attempt, as others have (Redfield, 1948; Craig and Hayward, 1987; Emerson *et al.,* 1991), to determine the relative importance of thermal and biological effects in surface waters, where the phasing of both is the same. In some regions, however, the nature of the cycles in our analyses is relatively clear. For example, we show that deeper tropical cycles are mainly physically-driven, an artifact of the adiabatic movement of the thermocline. Also, the correlation between the nodal depth and the compensation depth in middle and high latitudes strongly suggests the dominance of the annual cycle by biological processes above and below the nodal depth. Clearly, the continued use of models and other data sets will help to sort out the dominant processes that are responsible for the annual cycles of oxygen in the World Ocean.

We anticipate that our climatology will be useful for constraining global oxygen and carbon budgets and for evaluating numerical models of carbon and oxygen cycling in the atmosphere and the ocean. For example, the techniques pioneered by Schulenberger and Reid (1981), Jenkins and Goldman (1985) and Emerson (1987) for estimating new production could be attempted on a larger scale. As suggested by Keeling *et al.* (1993), air-sea fluxes of oxygen play a major role in the variability of atmospheric oxygen. Indeed, there is consistency between our surface analyses and seasonal variations in atmospheric $O_2/N_2$ (which are thought to be dominated by changes in $O_2$) in that atmospheric $O_2/N_2$ increases most rapidly in the summer when surface waters are most supersaturated, and decreases most rapidly in winter when surface waters are most undersaturated (Keeling and Shertz, 1992; Bender *et al.,* 1996). It seems likely that studies combining oceanic and atmospheric oxygen data will yield greater insight into global-scale carbon and oxygen cycling than separate analysis of the individual data sets.

The annual cycle is a dominant mode of variability in the biology and chemistry of the ocean. Until recently, studies of the seasonal variability of marine biogeochemical systems were limited to coastal regions and a few open ocean sites, constraining our ability to determine rates of a variety of marine biogeochemical processes on the global scale. Our global climatology of the annual cycle of the dissolved oxygen anomaly, and the recently-created global climatologies of the annual cycle of surface chlorophyll (Yoder *et al.,* 1993), primary productivity (Antoine *et al.,* 1996) and surface ocean $pCO_2$ (Takahashi *et al.,* 1996), should help to remedy this situation, and further our understanding of marine biogeochemistry on the global scale.

*Acknowledgments.* This work was initiated while the authors were postdoctoral fellows in the Advanced Study Program at the National Center for Atmospheric Research (sponsored by the National Science Foundation). We are thankful for the superb programming support of Gary Strand and Chuck Reich. We are grateful to Steve Worley for his assistance in the unpacking and initial processing of the NODC data. The comments of two anonymous reviewers were helpful in making the paper clearer. This work was supported by NASA grant 2383-MDIS/BGE005.

## APPENDIX

### Data processing

Here we describe in detail the process we used to create gridded, monthly-mean maps of the oxygen anomaly at various standard depths from discrete measurements of temperature, salinity and oxygen archived at the NODC.

*a. Vertical interpolation of temperature, salinity and oxygen.* The depth levels we used for the vertical interpolation of the temperature, salinity and oxygen observations are the 30 standard depth levels selected by the NODC plus the three levels added by Levitus (1982). The shallowest depth level is at the ocean surface and the deepest is at 5500 m. The distance between levels varies from 10 m at the surface to 500 m in the deep ocean. In order to prevent spurious extrema while maintaining maximum accuracy, we interpolated the data using the monotonic scheme of Steffen (1990). This is a *local* method, in which a cubic polynomial is fitted through each pair of adjacent points, the derivatives being determined at the points to insure that spurious extrema are not produced. Only those interpolated values that have one point above and one point below the standard level within an acceptable depth range of that standard level were retained. These ranges are the same as those chosen by Levitus *et al.* (1993), and are approximately twice the distance between levels. The top level, which is at 0 m, was treated differently: the value at this level was simply set equal to the shallowest value above 10 m.

*b. Calculating the oxygen anomaly.* From the vertically-interpolated temperature, salinity and oxygen observations, we computed the oxygen anomaly at standard pressure using

$$\Delta[O_2]^o = [O_2] - [O_2]^o_{sat},$$

where $[O_2]$ is the oxygen concentration of the water parcel and $[O_2]^o_{sat}$ is the concentration the water parcel would obtain if brought to the surface adiabatically and equilibrated with air at one atmosphere pressure and 100% relative humidity. Before computing the oxygen anomaly, we converted the oxygen concentration from ml $l^{-1}$ (which are the units used by NODC) to μmol $kg^{-1}$ using the molar volume of oxygen at STP and standard formulae for the potential density of seawater. The oxygen saturation concentration was computed using the formula of Garcia and Gordon (1992) at the potential temperature of the water parcel, also computed using standard formulae.

*c. Filtering the oxygen anomaly.* The oxygen measurements in the NODC archives were made by many scientists from a variety of institutions and countries throughout the past century. Because these data are of highly variable quality, a filtering procedure was devised to eliminate erroneous data. Because the size of the data set precluded a station-by-station manual inspection, an automated scheme was developed. Many investigators faced with similar tasks have statistically filtered the data by computing means and standard deviations on a coarse grid, and eliminating those observations more than several standard deviations from the mean. Our initial attempts using this technique showed a preference for eliminating observations near the edges of the coarse grid boxes, and so we chose not to use this type of filtering scheme.

A visual inspection of many of our preliminary maps revealed that if a measurement appeared erroneous, measurements from the whole cruise were often erroneous. We therefore developed a technique for evaluating the oxygen data on a cruise-by-cruise basis by comparing cruises of uncertain quality with a high quality subset of the NODC archives. If the comparison was good, this cruise was also considered to be of high quality; those cruises that did not compare favorably were rejected. In this way, we "grew" a high quality data set from a few seed cruises that consisted of 1208 stations among 27 cruises from the GEOSECS, TTO, TATO and SAVE programs. The comparison was at first restricted to measurements deeper than 2000 m where temporal and spatial variability is relatively weak. The internal consistency of our seed data set was evaluated by computing the RMS difference of the oxygen anomaly at 2000 m and deeper between each pair of stations within the data set. We found, not surprisingly, that the RMS difference increased with increasing distance between stations (Fig. A1). For the remaining cruises, the RMS difference was computed between the seed data set and those stations of a cruise that were within 50 km of our high quality stations. If five or more observations were compared, we passed the cruise if the RMS difference was less than a critical value; we failed the cruise if the RMS difference was greater than the critical value. We chose the critical value (5 μmol $kg^{-1}$) from Figure A1 by finding the value at which 10% of the comparisons within 50 km of five or more observations are greater than that critical value.

The passed cruises were then included into our high quality subset and the procedure was iterated until it converged and no more cruises could be evaluated. This procedure was able to evaluate only 42% of the stations among those at which the oxygen anomaly could

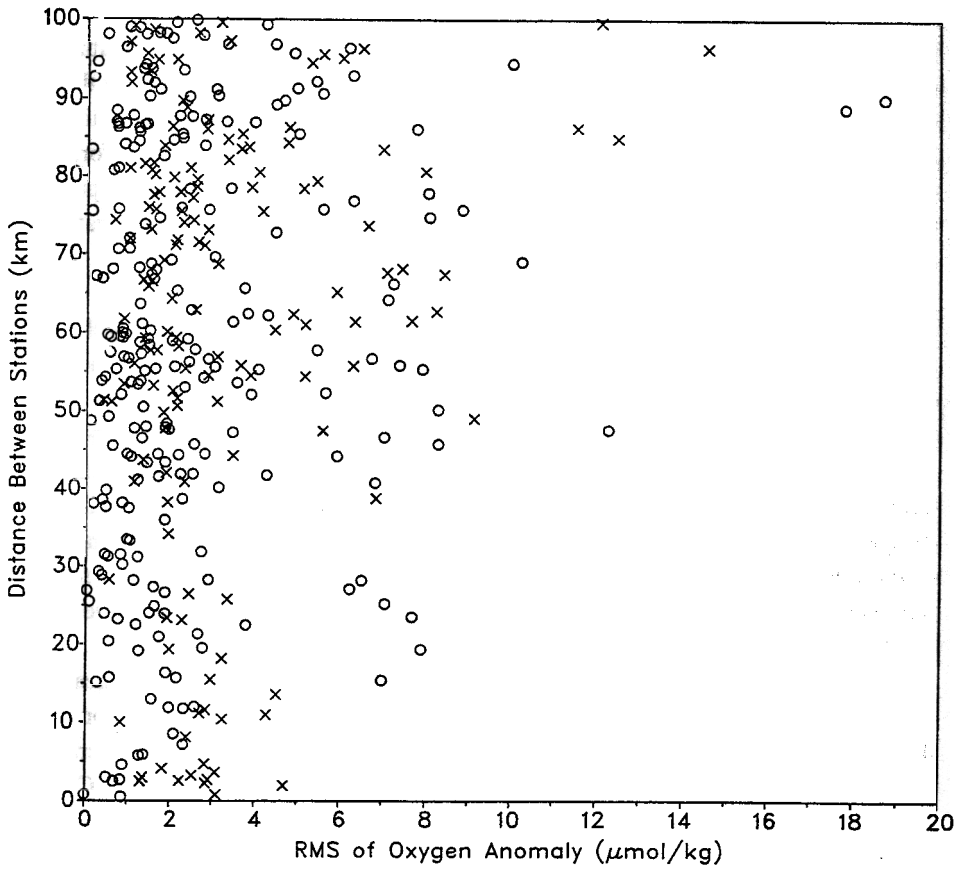


Figure A1. RMS difference of the oxygen anomaly below 2000 m between stations in the seed data set as a function of distance between stations. A circle indicates that the difference was computed from five or more depth levels; × indicates one to four depth levels.

be defined, presumably because most of the stations in the data set are in shallow nearshore waters (Fig. 2). We thus evaluated the remaining cruises based on observations below 1000 m; a 12 μmol $kg^{-1}$ cutoff was chosen based on the same criterion used for 2000 m. We finally repeated the procedure at 500 m, using a cutoff of 15 μmol $kg^{-1}$. Overall, we were able to evaluate 73% of the stations that contained a value of the oxygen anomaly.

Instead of eliminating all of the "failed" cruises—which would have trimmed the data set to such an extent that the annual cycle would have been poorly defined—we only eliminated those which were particularly bad: the worst 10% (in terms of the RMS difference) of the cruises that failed on each of the three passes through the scheme.

The filtered data set generated by this procedure generally yields more consistent patterns of variability than the unfiltered data, suggesting that the procedure indeed mostly rejected data of inferior quality. We cannot be sure that this was always the case, however.

For the North Indian Ocean, for example, the unfiltered data set actually reveals clearer, more consistent patterns than the filtered data (see Fig. 16). Except where noted, the filtered data set is used for the analysis presented here. In our opinion, quality control is the aspect of this study that could stand the most improvement.

*d. Binning the oxygen anomaly.* We binned the oxygen anomaly, filtered as described above, onto a horizontal and temporal grid with monthly resolution. Realizing that the data density in many regions precludes full resolution of the annual cycle, we employed a scheme in these regions for assigning a value of the oxygen anomaly based on coarser temporal resolution (see below). To resolve basin scale features on the order of 1000 km, we chose a horizontal resolution of approximately 200 km (about 2° in latitude) using a grid that is very nearly equal-area: 2° in latitude and variable in longitude, increasing from 2° at the equator to 120° at the poles (Rossow and Garder, 1984). Transformation to the common equal-angle grid is simple (Rossow and Garder, 1984). The grid can be seen in all of our horizontal plots (e.g., Fig. 2). For each depth level, we binned and averaged the oxygen anomaly by month onto the equal-area grid. We refer to these unevenly distributed fields as *binned* data.

*e. Interpolating and smoothing the oxygen anomaly.* There are a large variety of techniques for producing gridded maps from discrete observations (objective analysis). We employed a scheme in which the estimated value at a given grid point is essentially the distance-weighted average of surrounding observations. More sophisticated versions of this type were considered, such as optimal interpolation and iterative-correction, but these can produce spurious extrema, such as negative values in positive-definite quantities.

In the chosen scheme, the objectively-analyzed value at a given grid box for a given month is computed to be the distance-weighted average of the binned data at the given depth and month within a horizontal radius of influence, but only if five or more grid boxes within the radius of influence have data. The weight is given by the simple and frequently-used Cressman function (Cressman, 1959):

$$\omega(s) = \frac{d^2 - s^2}{d^2 + s^2}, \tag{A2}$$

where $d$ is the radius of influence (chosen to be 1000 km) and $s$ is the distance between the grid box for which the average is being computed and a binned data point. In employing the algorithm, we did not allow the radius of influence to cross the Isthmus of Panama or the Bering Strait region. Finally, inland seas were not included in our analysis. Thus, observations of the oxygen anomaly in the following waters were ignored: the Red Sea, the Persian Gulf, the Mediterranean Sea, the Black Sea, the Caspian Sea, the Baltic Sea, the White Sea and Hudson Bay. We refer to the fields produced by distance-weighted averaging as *mapped or objectively-analyzed* data.

In regions where the data density is very low, a distance-weighted average could not be

computed directly from the monthly binned data. We filled these regions with a three month average, computed as follows. From the monthly binned data, a three-month running average was computed, and the distance-weighted averaging scheme was applied to these new binned data to produce a new set of monthly maps. Even for these maps, there were some regions for which a value could not be computed, and so here we defaulted to a five-month map, computed similar to the three-month maps. For the five-month maps, it was possible to compute a value at almost every grid point. For the few remaining grid points, the distance-weighted scheme was applied to the five-month mapped data. In short, we were able to extract monthly resolution where possible, and defaulted to three- and then five-month running means where necessary. Finally, the monthly maps were smoothed with the Cressman function to eliminate discontinuities between regions where the one-, three- and five-month averages were used.

*f. Pressure correction for the surface oxygen anomaly.* We prepared two different sets of surface oxygen anomaly maps. One set was prepared as described above, based on a constant total atmospheric pressure of one atmosphere. This set of maps was then adjusted for climatological sea level pressure variations to produce a second set of maps according to:

$$\Delta[O_2] = \Delta[O_2]^o + \left(1 - \frac{p}{p^o}\right)[O_2]^o_{sat}, \tag{A3}$$

where $p$ is sea level pressure from Oberhuber (1988), $p^o$ is the mean sea level pressure (1013.25 mb), and $[O_2]^o_{sat}$ is computed from the temperature and salinity atlases of Levitus and Boyer (1994b) and Levitus *et al.* (1994). The average effect of the correction over a year is to make the oxygen anomaly greater in the polar and tropical regions and smaller in the subtropics. The effect is most pronounced in the Southern Hemisphere: the annual mean sea level pressure is about 2% lower at 60S than it is at 30S (Oberhuber, 1988), amounting to a change of about 5 μmol $kg^{-1}$ in the saturation concentration. With respect to seasonal variations, the correction is effectively limited to middle and high latitudes, where it makes the amplitude of the annual cycle of $\Delta[O_2]$ slightly smaller than that of $\Delta[O_2]^o$.

## REFERENCES

Antoine, D., J.-M. André and A. Morel. 1996. Oceanic primary production, 2, Estimation at global scale from satellite (coastal zone color scanner) chlorophyll. Global Biogeochem. Cycles, *10,* 57–70.

Baker, K. S. and R. Frouin. 1987. Relation between photosynthetically available radiation and total insolation at the ocean surface under clear skies. Limnol. Oceanogr., *32,* 1370–1377.

Bender, M., T. Ellis, P. Tans, R. Francey and D. Lowe. 1996. Variability in the $O_2/N_2$ ratio of southern hemisphere air: Implications for the carbon cycle. Global Biogeochem. Cycles, *10,* 9–21

Berger, W. H., K. Fischer, C. Lai and G. Wu. 1987. Ocean productivity and organic carbon flux. Part I: Overview of maps of primary production and export production, SIO Reference Series. Scripps Inst. of Oceanography, University of California, San Diego.

Bingham, F. M. and R. Lukas. 1996. Seasonal cycles of temperature, salinity and dissolved oxygen observed in the Hawaii Ocean time-series. Deep-Sea Res. II, *43,* 199–213.

Clarke, G. L. 1936. Light penetration in the western North Atlantic and its application to biological problems. Cons. Int. Explor. Mer, *101,* 14 pp.

Conkright, M. E., S. Levitus and T. P. Boyer. 1994. NOAA Atlas NESDIS 2, World Ocean Atlas 1994, Volume 1: Nutrients. U.S. Government Printing Office, Washington, D.C., 150 pp.

Craig, H. and T. Hayward. 1987. Oxygen supersaturation in the ocean: Biological versus physical contributions. Science, *235,* 199–202.

Cressman, G. P. 1959. An operational objective analysis system. Mon. Weath. Rev., *87,* 367–374.

Emerson, S. 1987. Seasonal oxygen cycles and biological new production in surface waters of the Subarctic Pacific Ocean. J. Geophys. Res., *92,* 6535–6544.

Emerson, S., P. Quay, C. Stump, D. Wilbur and M. Knox. 1991. $O_2$, Ar, $N_2$ and $^{222}Rn$ in surface waters of the Subarctic Ocean: Net biological $O_2$ production. Global Biogeochem. Cycles, *5,* 49–69.

Emerson, S., P. Quay, C. Stump, D. Wilbur and R. Schudlich. 1993. Determining primary production from the mesoscale oxygen field. ICES Mar. Sci. Symp., *197,* 196–206.

Garcia, H. E. and L. I. Gordon. 1992. Oxygen solubility in seawater: Better fitting equations. Limnol. Oceanogr., *37,* 1307–1312.

Gordon, A. L. 1986. Interocean exchange of thermocline water. J. Geophys. Res., *91,* 5037–5046.

Hayward, T. L. 1994. The shallow oxygen maximum layer and primary production. Deep-Sea Res., *41,* 559–574.

Jenkins, W. J. 1982. On the climate of a subtropical ocean gyre: Decade timescale variations in water mass renewal in the Sargasso Sea. J. Mar. Res., *40* (Suppl.), 265–290.

Jenkins, W. J. and J. C. Goldman. 1985. Seasonal oxygen cycling and primary production in the Sargasso Sea. J. Mar. Res., *43,* 465–491.

Keeling, R. F., R. G. Najjar, M. L. Bender and P. P. Tans. 1993. What atmospheric oxygen measurements can tell us about the global carbon cycle. Global Biogeochem. Cycles, *7,* 37–67.

Keeling, R. F. and S. R. Shertz. 1992. Seasonal and interannual variations in atmospheric oxygen and implications for the global carbon cycle. Nature, *358,* 723–727.

Kumar, S. P. and A. S. Unnikrishnan. 1995. Seasonal cycle of temperature and associated wave phenomena in the upper layers of the Bay of Bengal. J. Geophys. Res., *100,* 13585–13593.

Langdon, C., J. Marra and C. Knudson. 1995. Measurements of net and gross $O_2$ production, dark $O_2$ respiration, and $^{14}C$ assimilation at the Marine Light-Mixed Layers Site (59°N, 21°W) in the northeast Atlantic Ocean. J. Geophys. Res., *100,* 6645–6653.

Levitus, S. 1982. Climatological Atlas of the World Ocean, NOAA Prof. Pap. 13, U.S. Government Printing Office, Washington, D.C., 173 pp.

Levitus, S. and T. P. Boyer. 1994a. NOAA Atlas NESDIS 2, World Ocean Atlas 1994, Volume 2: Oxygen. U.S. Government Printing Office, Washington, D.C., 186 pp.

—— 1994b. NOAA Atlas NESDIS 2, World Ocean Atlas 1994, Volume 4: Temperature. U. S. Government Printing Office, Washington, D. C., 117 pp.

Levitus, S., R. Burgett, T. P. Boyer. 1994. NOAA Atlas NESDIS 2, World Ocean Atlas 1994, Volume 3: Salinity. U. S. Government Printing Office, Washington, D. C., 99 pp.

Levitus, S., J. L. Reid, M. E. Conkright, R. G. Najjar and A. Mantyla. 1993. Distribution of phosphate, nitrate and silicate in the world oceans. Prog. Oceanogr., *31,* 245–273.

Merle, J. 1983. Seasonal variability of subsurface thermal structure in the tropical Atlantic Ocean, *in* Hydrodynamics of the Equatorial Ocean, J. C. J. Nihoul, ed., Elsevier, Amsterdam, 31–49.

Meyers, G. 1975. Seasonal variation in transport of the Pacific North Equatorial Current relative to the wind field. J. Phys. Oceanogr., *5,* 442–449.

—— 1979. On the annual Rossby wave in the tropical North Pacific Ocean. J. Phys. Oceanogr., *9,* 663–674.

Michaels, A. F., A. H. Knap, R. L. Dow, K. Gundersen, R. J. Johnson, J. Sorensen, A. Close, G. A. Knauer, S. E. Lohrenz, V. A. Asper, M. Tuel and R. Bidigare. 1994. Seasonal patterns of ocean biogeochemistry at the U. S. JGOFS Bermuda Atlantic Time-series Study site, Deep-Sea Res, *41,* 1013–1038.

Morel, A. 1988. Optical modeling of the upper ocean in relation to its biogenous matter content (Case 1 waters). J. Geophys. Res., *93,* 10,749–10,768.

Morel, A. and R. C. Smith. 1982. Terminology and units in optical oceanography. Mar. Geodesy, *5,* 335–349.

Oberhuber, J. 1988. An atlas based on the COADS data set: The budgets of heat, buoyancy and turbulent kinetic energy at the surface of the global ocean. Max Planck Inst. für. Met. Rep. No. 15, Hamburg, Germany.

Okubo, A. 1959. An estimation of the average compensation depth by a study of the vertical distribution of dissolved oxygen. Rec. Oceanogr. Works Japan, *5,* 51–59.

Parsons, T. R., M. Takahashi and B. Hargrave. 1984. Biological Oceanographic Processes. Pergamon Press, Oxford, 330 pp.

Peng, T.-H., T. Takahashi, W. S. Broecker and J. Olafsson. 1987. Seasonal variability of carbon dioxide, nutrients and oxygen in the northern North Atlantic surface water: observations and a model. Tellus, *39B,* 439–458.

Platt, T., D. F. Bird and S. Sathyendranath. 1991. Critical depth and marine primary production. Proc. R. Soc. Lond. B, *246,* 205–217.

Rakestraw, N. W. and D. E. Carritt. 1948. Some seasonal chemical changes in the open ocean. J. Mar. Res., *7,* 362–369.

Raymont, J. E. G. 1980. Plankton and Productivity in the Oceans, Volume 1: Phytoplankton. Pergamon Press, Oxford, 489 pp.

Redfield, A. C. 1948. The exchange of oxygen across the sea surface. J. Mar. Res., *7,* 347–361.

Reid, J. L. 1962. Distribution of dissolved oxygen in the summer thermocline. J. Mar. Res., *20,* 138–148.

Reverdin, G. 1987. The upper equatorial Indian Ocean: The climatological seasonal cycle. J. Phys. Oceanogr., *17,* 903–927.

Richards, F. A. 1957. Oxygen in the ocean. Geol. Soc. Amer. Memoir *57,* 1, 185–238.

Ropelewski, C. F. 1989. Monitoring large-scale cryosphere/atmosphere interactions. Adv. Space Res., *9,* 213–218.

Rossow, W. B. and L. Garder. 1984. Selection of a map grid for data analysis and archival. J. Climate and Appl. Meteo., *23,* 1253–1257.

Shaw, P.-T., S.-Y. Chao, K.-K. Liu, S.-C. Pai and C.-T. Liu. 1996. Winter upwelling off Luzon in the northeastern South China Sea. J. Geophys. Res., *101,* 16435–16448.

Shea, D. J., K. E. Trenberth and R. W. Reynolds. 1992. A global monthly sea surface temperature climatology. J. Climate, *5,* 987–1001.

Shulenberger, E. and J. L. Reid. 1981. The Pacific shallow oxygen maximum, deep chlorophyll maximum, and primary productivity, reconsidered. Deep-Sea Res., *28,* 901–919.

Smetacek, V. and U. Passow. 1990. Spring bloom initiation and Sverdrup's critical-depth model. Limnol. Oceanogr., *35,* 228–234.

Spitzer, W. S. and W. J. Jenkins. 1989. Rates of vertical mixing, gas exchange and new production: Estimates from seasonal gas cycles in the upper ocean near Bermuda. J. Mar. Res., *47,* 169–196.

Stefánsson, U. and F. A. Richards. 1964. Distributions of dissolved oxygen, density, and nutrients off the Washington and Oregon coasts. Deep-Sea Res., *11,* 355–380.

Steffen, M. 1990. A simple method for monotonic interpolation in one dimension. Astron. Astrophys., *239,* 443–450.

Suga, T. and K. Hanawa. 1990. The mixed-layer climatology in the northwestern part of the North Pacific subtropical gyre and the formation area of Subtropical Mode Water. J. Mar. Res., *48,* 543–566.

Sverdrup, H. U. 1953. On conditions for the vernal blooming of phytoplankton. J. Cons. Perm. Int. Exp. Mer., *18,* 287–295.

Tabata, S. 1965. Variability of oceanographic conditions at Station "P" in the Northeast Pacific Ocean. Trans. Royal Soc. Canada, *3,* 367–418.

Takahashi, T., R. A. Feely, R. Weiss, R. H. Wanninkhof, D. W. Chipman, S. C. Sutherland and T. T. Takahashi. 1996. Global air-sea flux of $CO_2$: An estimate based on measurements of the sea-air $pCO_2$ difference, Proceedings of the National Academy of Science (Revelle Colloquium), (submitted).

Tomczak, M. and S. Godfrey. 1994. Regional Oceanography: An Introduction. Pergamon Press, Oxford, England, 422 pp.

White, W. B. 1978. A wind-driven model experiment of the seasonal cycle of the main thermocline in the interior midlatitude North Pacific. J. Phys. Oceanogr., *8,* 818–824.

Worthington, L. V. 1959. The 18° water in the Sargasso Sea. Deep-Sea Res., *5,* 297–305.

Wyrtki, K. 1961. Physical Oceanography of the Southeast Asian Waters. NAGA Report: Volume 2. Scientific Results of the Marine Investigations of the South China Sea and Gulf of Thailand, 1959–1961. University of California, Scripps Institution of Oceanography, La Jolla, California, 195 pp.

- 1981. An estimate of equatorial upwelling in the Pacific. J. Phys. Oceanogr., *11,* 1205–1214.

Yoder, J. A., C. R. McClain, G. C. Feldman and W. E. Esaias. 1993. Annual cycles of phytoplankton chlorophyll concentrations in the global ocean: A satellite view. Global Biogeochem. Cycles, *7,* 181–194.

Received: *23 April, 1996;* revised: *24 September, 1996.*